Intensity-invariance of fine time structure in basilar-membrane click responses: Implications for cochlear mechanics

Christopher A. Shera[a)]
Eaton-Peabody Laboratory of Auditory Physiology, Massachusetts Eye and Ear Infirmary, 243 Charles Street, Boston, Massachusetts 02114 and Department of Otology and Laryngology, Harvard Medical School, Boston, Massachusetts 02115

(Received 31 January 2001; accepted for publication 16 April 2001)

Basilar-membrane and auditory-nerve responses to impulsive acoustic stimuli, whether measured directly in response to clicks or obtained indirectly using cross- or reverse-correlation and/or Fourier analysis, manifest a striking symmetry: near-invariance with stimulus intensity of the fine time structure of the response over almost the entire dynamic range of hearing. This paper explores the origin and implications of this symmetry for cochlear mechanics. Intensity-invariance is investigated by applying the EQ-NL theorem [de Boer, Aud. Neurosci. **3**, 377–388 (1997)] to define a family of linear cochlear models in which the strength of the active force generators is controlled by a real-valued, intensity-dependent parameter, γ (with $0 \leqslant \gamma \leqslant 1$). The invariance of fine time structure is conjectured to imply that as γ is varied the poles of the admittance of the cochlear partition remain within relatively narrow bands of the complex plane oriented perpendicular to the real frequency axis. Physically, the conjecture implies that the local resonant frequencies of the cochlear partition are nearly independent of intensity. Cochlear-model responses, computed by extending the model obtained by solution of the inverse problem in squirrel monkey at low sound levels [Zweig, J. Acoust. Soc. Am. **89**, 1229–1254 (1991)] with three different forms of the intensity dependence of the partition admittance, support the conjecture. Intensity-invariance of cochlear resonant frequencies is shown to be consistent with the well-known ''half-octave shift,'' describing the shift with intensity in the peak (or best) frequency of the basilar-membrane frequency response. Shifts in best frequency do not arise locally, via changes in the underlying resonant frequencies of the partition, but globally through the intensity dependence of the driving pressure. Near-invariance of fine time structure places strong constraints on the mechanical effects of force generation by outer hair cells. In particular, the symmetry requires that the feedback forces generated by outer hair cells (OHCs) not significantly affect the natural resonant frequencies of the cochlear partition. These results contradict many, if not most, cochlear models, in which OHC forces produce significant changes in the reactance and resonant frequencies of the partition.
 [DOI: 10.1121/1.1378349]

PACS numbers: 43.64.Bt, 43.64.Kc, 43.66.Ba [LHC]

I. INTRODUCTION

Responses of the basilar membrane and auditory nerve to acoustic clicks reveal a striking symmetry: near-invariance with stimulus intensity of the fine time structure of the response over almost the entire dynamic range of hearing. In measurements of basilar-membrane motion the symmetry appears as a near-invariance of the zero crossings of the mechanical waveform (e.g., Robles *et al.*, 1976; Ruggero *et al.*, 1992; de Boer and Nuttall, 1997; Recio *et al.*, 1998; Recio and Rhode, 2000). In the auditory nerve, the invariance is manifest at low and moderate sound levels in the approximate level independence of the latency to the peaks of both standard poststimulus-time (PST) and recovered-probability compound PST histograms (e.g., Kiang *et al.*, 1965; Goblick and Pfeiffer, 1969; Lin and Guinan, 2000).[1] Intensity-invariance of fine temporal detail is remarkably robust to the method of measurement: The symmetry appears in (1) direct measurements of mechanical and neural ''impulse responses'' obtained using acoustic clicks; (2) indirect estimates obtained by cross- or reverse-correlation using wideband noise stimuli (e.g., Carney and Yin, 1988; Carney *et al.*, 1999; de Boer and Nuttall, 1997, 2000); and (3) ''synthetic'' time-domain waveforms obtained by applying inverse Fourier analysis to frequency-domain transfer functions measured with pure tones (e.g., Recio and Rhode, 2000).

Figure 1 illustrates the near intensity-invariance of fine time structure using recent measurements of basilar-membrane (BM) click responses in chinchilla (Recio and Rhode, 2000). Although the envelopes of the response waveforms shift systematically with stimulus intensity over the 70 dB range represented in the figure, the timings of the peaks, valleys, and zero crossings remain almost unchanged. The problem of understanding the origin of this symmetry has been nicely highlighted by de Boer and Nuttall (2000). Seeking to identify necessary and sufficient conditions for obtaining the symmetry, they applied the ''EQ-NL theorem'' (de Boer, 1997) to study the intensity dependence of basilar-membrane motion in the guinea pig. Although they derived a

a)Electronic mail: shera@epl.meei.harvard.edu

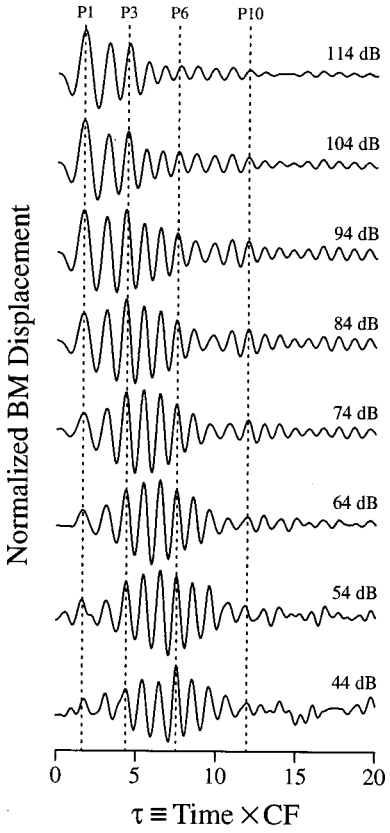

FIG. 1. Near-invariance of fine time structure in basilar-membrane click responses. The figure shows normalized BM responses to clicks from Recio and Rhode (2000, Fig. 2, chinchilla CB21). The horizontal axis measures time after the onset of umbo vibration in periods of the CF (14.5 kHz). Displacement waveforms are normalized to unit amplitude with peak click intensities indicated on the right in dB pSPL. The vertical dotted lines mark selected peaks in the response waveform (P1, P3, P6, and P10). Although the waveform envelopes vary systematically with click intensity (e.g., the envelope maximum shifts in time from about eight periods after the onset of middle-ear vibration at 44 dB pSPL to about two periods at 114 dB), the underlying fine time structure remains nearly invariant (e.g., the times of occurrence of the waveform peaks, valleys, and zero crossings generally vary by substantially less than a quarter period over the same intensity range). Adapted from Recio and Rhode (2000).

cochlear model—based on basilar-membrane impedance functions obtained from inverse analysis of measured cross-correlation functions—that exhibits the near-invariance of the timing of the mechanical impulse response, the origin and implications of the symmetry for cochlear mechanics have remained elusive.

This paper takes up the problem, adopting the modeling framework introduced in an earlier study of the frequency modulations (or ''glides'') evident in impulse responses of the basilar membrane and auditory nerve (Shera, 2001). Glides, which represent a change over time in the instantaneous frequency of oscillation of the response waveform, are nearly independent of stimulus intensity (e.g., de Boer and Nuttall, 1997; Recio *et al.*, 1998; Carney *et al.*, 1999; Recio and Rhode, 2000) and even maintain their general form post mortem (e.g., Recio *et al.*, 1998). The intensity-invariance of glides follows from the invariance of fine time structure we explore here. In an earlier paper (Shera, 2001), we demonstrated basic properties of glides, emphasizing their scaling behavior and their relation to the group delay of the frequency-domain transfer function. Here, we examine the implications for cochlear mechanics—and, in particular, for the mechanisms underlying cochlear amplification and dynamic-range compression—of the near intensity-invariance of the timing of the oscillations of mechanical and neural impulse responses. It might seem unlikely that one can learn much about the mechanisms of cochlear amplification from a phenomenon that appears to be largely independent of that amplification. That independence, however, is the key property: Whatever the outer hair cells are doing, they are doing it in a way that leaves the fine time structure of the impulse response invariant. Requiring this invariance turns out to place strong constraints on the mechanical effects of force generation by outer hair cells.

II. INVARIANCE OF BM RESONANT FREQUENCIES

A. Modeling framework

We adopt a simple modeling framework based on the classical point-impedance model of the cochlea. We assume that at sound intensities in the low-level linear regime near threshold, the velocity $V_{\rm BM}(x,f)$ of the basilar membrane at position x due to sinusoidal stimulation at frequency f can be written as the product of two factors:

$$V_{\rm BM}(x,f)=Y_{\rm BM}(x,f)P(x,f). \tag{1}$$

The first term, $Y_{\rm BM}(x,f)$, represents the admittance of the cochlear partition, and the second term, $P(x,f)$, represents the driving pressure difference across it. In the time domain, Eq. (1) becomes a convolution:

$$v_{\rm BM}(x,t)=y_{\rm BM}(x,t)*p(x,t), \tag{2}$$

where lower- and upper-case quantities (e.g., $v_{\rm BM}$ and $V_{\rm BM}$) are related by Fourier transformation. As noted in an earlier paper on glides (Shera, 2001), the admittance $y_{\rm BM}(x,t)$ and driving pressure $p(x,t)$ differ profoundly in character. The admittance term $y_{\rm BM}(x,t)$ characterizes the response of an isolated section of the cochlear partition to an impulsive force and depends only on the *local* properties of the partition at position x. The pressure term $p(x,t)$, by contrast, represents the driving force applied *in situ* and is therefore *global*; since stimuli are usually applied in the ear canal (or, effectively, at the stapes when responses are normalized by stapes motion) and must propagate to the measurement location, $p(x,t)$ depends not only on the form of the stimulus, but also on the mechanics of the entire cochlea, including boundary conditions at the stapes and helicotrema.

We simplify the discussion by assuming the approximate local scaling symmetry (Zweig, 1976; Siebert, 1968; Sondhi, 1978) manifest by basilar-membrane transfer functions (Rhode, 1971; Gummer *et al.*, 1987) and neural tuning curves (e.g., Kiang and Moxon, 1974; Liberman, 1978). Local scaling symmetry implies that rather than depending on position and frequency independently, mechanical transfer functions and tuning curves in fact depend on the two variables f and x primarily in the dimensionless combination $\beta(x,f)\equiv f/f_{\rm CF}(x)$, where $f_{\rm CF}(x)$ is the CF at location x (i.e., the cochlear position-frequency map).[2] In the time domain, scaling implies that corresponding basilar-membrane and

neural impulse responses depend on t and x through the dimensionless combination $\tau(x,t) \equiv t f_{CF}(x)$ representing time measured in periods of the characteristic frequency. Data supporting this time-domain manifestation of scaling were presented in the earlier paper on glides (Shera, 2001). When rewritten in terms of the scaling variables β and τ, Eqs. (1) and (2) become

$$V_{BM}(\beta) = Y_{BM}(\beta) P(\beta)$$

and (3)

$$v_{BM}(\tau) = y_{BM}(\tau) * p(\tau).$$

B. Parametrizing the intensity dependence

The model impedance $Z_{BM}(\beta) \equiv 1/Y_{BM}(\beta)$ characterizes the motion of the cochlear partition at sound levels in the low-level linear regime near threshold. Preparatory to modeling the intensity dependence, we follow others (e.g., Neely, 1983; Zweig, 1990; de Boer and Nuttall, 2000) and write Z_{BM} in the form

$$Z_{BM}(\beta) = Z_p(\beta) + Z_a(\beta), \tag{4}$$

representing the sum of a ''passive'' and an ''active'' component. The impedance $Z_a(\beta)$ characterizes the local effect of force generation by outer hair cells (OHCs); the impedance $Z_p(\beta)$ characterizes the mechanics of the partition obtained when those force generators have been disabled. This ''two-component'' form of the impedance is consistent with the experimental findings of de Boer and Nuttall, as reflected in their solutions to the inverse problem in guinea pig (de Boer and Nuttall, 2000). Note that the impedances are assumed to scale and are therefore written as functions of the scaling variable $\beta(x,f) = f/f_{CF}(x)$.

In the spirit of the EQ-NL theorem (de Boer, 1997) and its application in guinea pig (de Boer and Nuttall, 2000), we then model intensity dependence by defining a family of linear models in which the effective strength of the active force generators is parametrized by the factor γ:

$$Z_{BM}(\beta;\gamma) = Z_p(\beta) + \gamma Z_a(\beta), \tag{5}$$

where the real parameter γ satisfies $0 \leqslant \gamma \leqslant 1$ and depends on the amplitude of local basilar-membrane displacement, and thus, indirectly, on stimulus intensity. To indicate this dependence we write $\gamma = \gamma(I/I_0)$, where I is the intensity and I_0 a reference that sets the scale. In the low-level linear limit near threshold ($I \ll I_0$), γ is approximately 1, independent of I; at high intensities ($I \gg I_0$), γ approaches 0. At intermediate intensities, γ is presumed to vary monotonically between 1 and 0; its precise value at any given intensity depends on the form of the nonlinearity associated with the active force generators (e.g., the form of the saturating displacement–voltage transduction function of the OHC stereocilia).[3]

Each value of γ yields a corresponding linear model, $\mathcal{M}(\gamma)$. According to the EQ-NL theorem, the linear model $\mathcal{M}(\gamma)$ has the same input–output cross-correlation function as a nonlinear model in which (a) the low-level linear limit is described by $\mathcal{M}(1)$ [i.e., by Eq. (5) with $\gamma = 1$] and (b) the effect of increasing stimulus intensity is partially to saturate the active force generators (e.g., the OHCs), reducing their effective strength by the factor γ. The model $\mathcal{M}(0)$ thus describes the high-level linear limit (or postmortem condition) in which the active force generators have been entirely disabled. Application of the EQ-NL theorem to cochlear responses requires that the input–output cross-correlation functions be measured with flat-spectrum wideband noise (so that the same value of γ characterizes OHC saturation throughout the cochlea) and subsequently normalized by stapes velocity. The OHC transduction nonlinearity is assumed to be memoryless and instantaneous. For a full discussion, see de Boer (1997).

By applying the EQ-NL theorem, we have replaced the analysis of a single nonlinear model (difficult) with the analysis of a large number of linear models, one for each noise intensity (easier). Although the net result is a substantial simplification of the analysis, the substitution is valid only for quantities, such as cross-correlation functions, measured with wideband noise stimuli (de Boer, 1997). Note, however, that the phenomena we explore here—the intensity-invariance of fine time structure in mechanical and neural impulse responses—is robust to the measurement technique and is seen in derived impulse responses measured with noise stimuli (e.g., de Boer and Nuttall, 1997, 2000; Carney *et al.*, 1999).

C. Admittance poles of a simple oscillator

To probe the origin of the near-invariance of fine time structure in cochlear responses, we first consider a simpler example: the impulse response of an harmonic oscillator and its relation to the poles of the admittance in the complex plane. The admittance, Y_p, of a simple harmonic oscillator—such as the passive resonator later assumed to characterize the cochlear partition at high sound intensities—has the form

$$Y_p(f) \propto \frac{i f f_p}{f_p^2 - f^2 + i \delta_p f f_p}, \tag{6}$$

where f_p is the resonant frequency in the limit of zero damping and δ_p is the dimensionless damping constant. Introducing the normalized frequency $\beta = f/f_{CF}$ for future convenience, we now rewrite Eq. (6) to express Y_p in terms of the locations of its poles. Equation (6) becomes

$$Y_p(\zeta) \propto \frac{i \zeta \nu}{(\zeta - \zeta_\times)(\zeta - \zeta_\times^*)}, \tag{7}$$

where the normalized pole locations are denoted $\zeta_\times$ and $-\zeta_\times^*$, and the variable ζ represents the complex extension of the real variable β, defined so that ζ equals β along the real axis ($\beta = \mathrm{Re}\{\zeta\}$). The superscripted asterisk ($*$) denotes complex conjugation. The positive-frequency pole, at location $\zeta_\times$, has real and imaginary parts $\zeta_\times \equiv \beta_\times + i\alpha_\times$, where the constants $\alpha_\times = \nu \delta_p/2$ and $\beta_\times = \nu\sqrt{1 - (\delta_p/2)^2}$, with $\nu \equiv f_p/f_{CF} = |\zeta_\times|$.

Since the impulse response of the oscillator has the form $\sin(2\pi\beta_\times\tau) e^{-2\pi\alpha_\times\tau}$, where $\tau \equiv t f_{CF}$ is normalized time, we see that the real part of the pole location ($\beta_\times$) corresponds to the normalized natural frequency of oscillation and the imaginary part ($\alpha_\times$) to the decay constant of the envelope.

This correspondence implies that by varying $\alpha_\times$ while holding $\beta_\times$ fixed one generates a family of oscillators[4] whose impulse responses differ in their envelopes but maintain identical underlying frequencies of oscillation. In other words, moving the poles along lines perpendicular to the real frequency axis changes the envelope of the impulse response while preserving the fine time structure of the waveform.[5]

D. Conjecture

Analysis of the harmonic oscillator indicates that intensity-invariance of the impulse response timing corresponds to movement of the admittance poles along lines nearly perpendicular to the real frequency axis. Applying these ideas to the motion of the basilar membrane, we recall from Eq. (3) that the velocity impulse response, $v_{\mathrm{BM}}(\tau;\gamma)$, is the convolution of $p(\tau;\gamma)$ and $y_{\mathrm{BM}}(\tau;\gamma)$. Since $y_{\mathrm{BM}}(\tau;\gamma)$ depends on the analytic structure of the mechanical admittance, $Y_{\mathrm{BM}}(\beta;\gamma)$, in the complex plane, our results from the oscillator example would carry over immediately if the driving force producing the motion $v_{\mathrm{BM}}(\tau;\gamma)$ were a single impulse applied locally, as it is for the oscillator. In the cochlea, however, the driving force consists of the traveling pressure wave, $p(\tau;\gamma)$, whose dispersive character introduces additional time and frequency dependence (e.g., Shera, 2001). We note, however, that the traveling pressure wave is not independent of the mechanics of the partition; indeed, the pressure $p(\tau;\gamma)$ depends intimately on the spatial variation of the admittance, and the intensity dependence of $p(\tau;\gamma)$ is ultimately determined by that of $Y_{\mathrm{BM}}(\beta;\gamma)$. We therefore conjecture that our conclusions from the oscillator apply also to cochlear mechanics. In particular, we suggest that the near-invariance of fine time structure in BM impulse responses implies that the poles of the effective BM admittance remain within relatively narrow bands of the complex plane oriented perpendicular to the real frequency axis as the parameter γ (i.e., stimulus intensity) is varied. If our conjecture is correct, the natural resonant frequencies of the cochlear partition, defined by the real part of the admittance pole locations, must be nearly independent of intensity.

III. TESTING THE CONJECTURE

We now explore this conjecture using a simple model of cochlear mechanics. The model defined by Eq. (5) requires specification of two impedances. For later convenience—and because it corresponds with the procedure for estimating these impedances experimentally (e.g., Zweig, 1990; de Boer and Nuttall, 2000)—we take the two impedances to be those obtained (1) in the low-level linear limit [i.e., $Z_{\mathrm{BM}}(\beta;1)$] and (2) with the active mechanisms disabled [i.e., $Z_{\mathrm{BM}}(\beta;0)$]. Note that we can write $Z_{\mathrm{p}}(\beta)=Z_{\mathrm{BM}}(\beta;0)$ and $Z_{\mathrm{a}}(\beta)=Z_{\mathrm{BM}}(\beta;1)-Z_{\mathrm{p}}(\beta)$. Thus,

$$Z_{\mathrm{BM}}(\beta;\gamma)=Z_{\mathrm{p}}(\beta)+\gamma[Z_{\mathrm{BM}}(\beta)-Z_{\mathrm{p}}(\beta)], \tag{8}$$

where we define $Z_{\mathrm{BM}}(\beta)\equiv Z_{\mathrm{BM}}(\beta;1)$ as a notational shorthand. In the following sections we discuss our model forms for the low- and high-level impedances $Z_{\mathrm{BM}}(\beta)$ and $Z_{\mathrm{p}}(\beta)$ appearing in Eq. (8).

A. The impedance of the cochlear partition, $Z_{\mathrm{BM}}(\beta)$

To characterize the response of the cochlear partition in the low-level linear regime ($\gamma=1$), we adopt a variant of the model impedance obtained by solution of the inverse problem in the squirrel monkey (Zweig, 1991). We use this model both for its convenient analytic form and because it constitutes perhaps the simplest system that displays many of the qualitative features of the real cochlea. In the model, the BM impedance scales and has the form of an harmonic oscillator, with a net *negative* damping, stabilized by a feedback force proportional to the oscillator displacement at an earlier time. The model admittance has the form (Zweig, 1991)[6]

$$Y_{\mathrm{BM}}(\beta)\propto\frac{i\beta}{1-\beta^2+i\delta\beta+\rho e^{-2\pi i\mu\beta}}, \tag{9}$$

where the dimensionless parameter δ represents the net damping (with $\delta<0$); and the dimensionless parameters ρ and μ characterize, respectively, the strength and the time delay (in periods of the local resonant frequency) of the stabilizing feedback force.

The parameter values found by Zweig (1991) imply that the admittance $Y_{\mathrm{BM}}(\beta)$ has, among an infinite series of poles in the complex β (or ζ) plane, two closely spaced poles just above the real frequency axis near $\beta=1$.[7] By making both the impedance magnitude and its derivative small at frequencies near CF, the two closely spaced poles in $Y_{\mathrm{BM}}(\beta)$ help create the tall, broad peak of the transfer function (Zweig, 1990). The model variant used here has the same functional form as the original, but differs somewhat in its parameter values. By using slightly different parameter values, we can make the two closely spaced poles coincident without significant effect on the corresponding transfer function (Shera, 1992; Zweig and Shera, 1995). For ease of analysis, we use this simpler ''double-pole'' form of the admittance. The model parameter values are thus determined by specifying that the two poles principally responsible for the peak in the admittance near $\beta=1$ coincide at a given distance from the real frequency axis.[8] The parameter that sets this distance and the additional parameter, N, representing the approximate number of wavelengths of the traveling wave on the basilar membrane (Zweig *et al.*, 1976; Zweig, 1991)[9] were chosen in order to produce a BM velocity impulse response that peaks after about ten periods of the characteristic frequency (in rough agreement with data at low sound–pressure levels from guinea pig and chinchilla).

B. The passive impedance, $Z_{\mathrm{p}}(\beta)$

We take the impedance that characterizes the passive ($\gamma=0$) system, $Z_{\mathrm{p}}(\beta)$, to be a simple harmonic oscillator with positive damping.[10] This form is consistent with recent attempts to fit experimental data obtained from the basal turns of the cochlea in passive preparations (e.g., Mammano and Nobili, 1993; Brass, 2000). Initially, we take the resonant frequency characterizing the passive system (f_{p}) to have a value approximately equal to the local CF [i.e., $\nu=f_{\mathrm{p}}(x)/f_{\mathrm{CF}}(x)\approx 1$]. We explore the implications of this choice of resonant frequency in Sec. III D. To reflect the

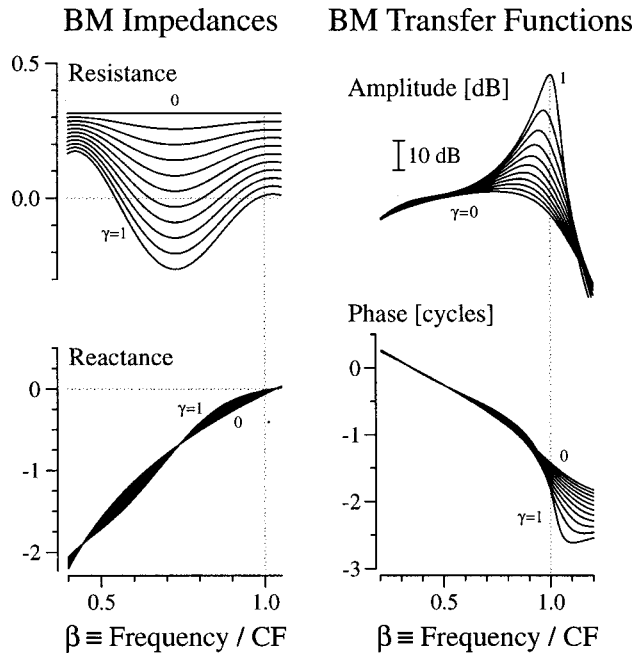

FIG. 2. Intensity dependence of BM impedances and velocity transfer functions for model $\mathcal{M}^{\approx}$. The left-hand panel shows the real (top) and imaginary parts (bottom) of the BM impedance $Z_{\mathrm{BM}}(\beta;\gamma)$ for eleven values of γ spanning the range 0–1 in steps of 0.1. Units are defined so that the proportionality constant in Eq. (9) for $Y_{\mathrm{BM}}(\beta)$ equals unity. The right-hand panel shows the amplitudes (top) and phases (bottom) of corresponding BM transfer functions, $T(\beta;\gamma)$. The dimensionless frequency variable $\beta \equiv f/f_{\mathrm{CF}}(x)$ increases along the abscissa. The vertical dotted lines locate the peak of the transfer function in the low-level linear limit ($\gamma=1$).

approximate equality of f_{p} and f_{CF}, we denote the model $\mathcal{M}^{\approx}$.[11] With functional forms now specified for both Z_{p} and Z_{BM}, the ''active impedance,'' Z_{a}, can be obtained by subtraction. Equation (8) allows us then to compute $Z_{\mathrm{BM}}(\beta;\gamma)$ as a function of γ by interpolating between these extremes.

C. Results for model $\mathcal{M}^{\approx}$

1. Transfer functions and impedances

Figure 2 shows the impedances $Z_{\mathrm{BM}}(\beta;\gamma)$ and corresponding BM transfer functions $T(\beta;\gamma)$ for values of γ spanning the full range [0,1]. The model transfer functions and impedances—both their form and their variation with intensity—bear a strong qualitative resemblance to those measured experimentally or obtained using the inverse method (cf. Figs. 2–4 of de Boer and Nuttall, 2000). For example, at the lowest effective intensity ($\gamma=1$), the real part of $Z_{\mathrm{BM}}(\beta;\gamma)$ is negative over an extended region of β just basal to the response peak at $\beta=1$. (In this description, we have used scaling to regard the figure as illustrating model impedances and transfer functions versus cochlear location at fixed frequency.[12]) The traveling wave is amplified as it propagates through the region of negative damping. At smaller values of γ (i.e., at higher intensities), $\mathrm{Re}\{Z_{\mathrm{BM}}(\beta;\gamma)\}$ increases towards 0, the region of amplification narrows, and the total gain decreases (as measured, for example, by the height of the transfer-function peak). As intensity increases further, the region of power amplification rapidly shrinks to zero and disappears (in this case, at $\gamma\approx 0.55$). Although the real part of the impedance then becomes everywhere positive, the influence of the active force generators in shaping the impedance remains evident at even the highest intensities. These changes in $\mathrm{Re}\{Z_{\mathrm{BM}}(\beta;\gamma)\}$ are accompanied by corresponding, although less dramatic, changes in the reactive component of the impedance. At all intensities the reactive component remains negative, resembling a stiffness, throughout the region of the transfer-function peak ($\beta<1.03$).[13] Note that the changes in $\mathrm{Im}\{Z_{\mathrm{BM}}(\beta;\gamma)\}$, as with those in $\mathrm{Re}\{Z_{\mathrm{BM}}(\beta;\gamma)\}$, depend strongly on location and frequency. Near the peak the cochlear amplifier acts to reduce the effective stiffness, and this reduction diminishes at higher intensities; thus, changes in $\mathrm{Im}\{Z_{\mathrm{BM}}(\beta;\gamma)\}$ are such that the effective stiffness, like the effective damping, increases with intensity.

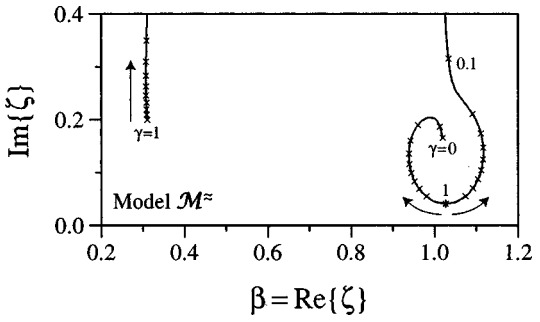

FIG. 3. Admittance pole trajectories for model $\mathcal{M}^{\approx}$. The figure shows trajectories in the ζ plane of the principal positive-frequency poles of $Y_{\mathrm{BM}}(\zeta;\gamma)$ for model $\mathcal{M}^{\approx}(\gamma)$ as a function of γ. At $\gamma=1$, $Y_{\mathrm{BM}}(\zeta;\gamma)$ has a double pole (*) at $\zeta_{*}\approx 1.03+i0.04$. As γ decreases the two poles separate slightly and move out along the solid lines in the directions shown by the arrows. Markers ($\times$) measure off equal intervals of γ spanning the range 0–1 in steps of 0.1. A third pole near $\mathrm{Re}\{\zeta\}=0.3$ contributes to shaping the ''tail'' of the transfer function. In the limit $\gamma\to 0$, all but one of the poles move off towards infinity, and the admittance $Y_{\mathrm{BM}}(\zeta;\gamma)$ becomes a passive harmonic oscillator, $Y_{\mathrm{p}}(\zeta)$, characterized by a single pole at $\zeta\approx 1.03+i0.17$.

2. Admittance pole trajectories

Figure 3 shows the locations of the principal, positive-frequency poles of the model-$\mathcal{M}^{\approx}$ BM admittance, $Y_{\mathrm{BM}}(\zeta;\gamma)$, as a function of γ. [By principal poles we mean those whose projection onto the real frequency axis falls near or below CF (i.e., $|\beta_{\times}|\lesssim 1$, where $\beta_{\times}=\mathrm{Re}\{\zeta_{\times}\}$). The remaining poles, located substantially above CF,[14] are less important in shaping the peak of the transfer function.] The lines trace out the trajectories of the principal poles as γ is decreased from 1 towards 0. For $\gamma=1$ (i.e., in the low-level linear limit), two poles coincide close to the real axis near $\mathrm{Re}\{\zeta\}=1.03$. Coincident poles are shown with an asterisk (*). A third pole near $\mathrm{Re}\{\zeta\}=0.3$ contributes to shaping the ''tail'' of the transfer function. In addition to these three principal poles (and their counterparts in the negative-frequency half plane), $Y_{\mathrm{BM}}(\zeta;\gamma)$ has an infinite string of poles at higher values of $\mathrm{Re}\{\zeta\}$ (Zweig, 1991). Note that the two coincident poles occur slightly above CF at a value $\beta_{*}=\mathrm{Re}\{\zeta_{*}\}\approx 1.03$ greater than 1. This value of β locates the normalized natural ''resonant frequency'' of an isolated section of the cochlear partition and corresponds closely to the point in Fig. 2 where the imaginary part of $Z_{\mathrm{BM}}(\beta;\gamma)$ crosses the zero line.

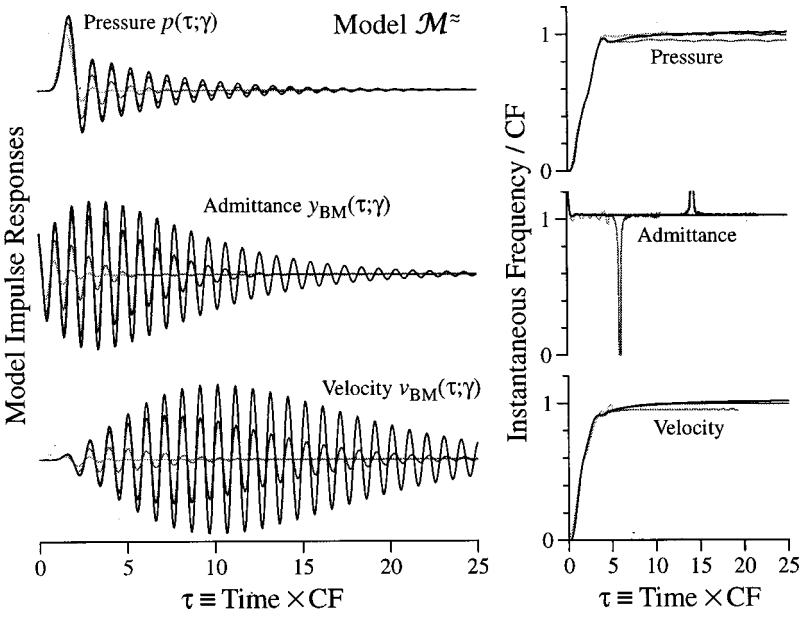

FIG. 4. Impulse responses and their instantaneous-frequency trajectories for several values of γ in model $\mathcal{M}^{\approx}$. The figure shows impulse responses (left) and corresponding instantaneous-frequency (IF) trajectories (right) for model pressure, admittance, and velocity responses (top to bottom, respectively). Responses are shown as a function of the dimensionless time variable $\tau \equiv t f_{CF}(x)$ for $\gamma = \{1,0.95,0.7,0\}$, with darker lines indicating larger values of γ (i.e., lower intensities). IF trajectories were computed as described elsewhere (Shera, 2001). The sharp notches apparent in the IF trajectory for $y_{BM}(\tau;\gamma)$ (e.g., near $\tau \approx 14$ for $\gamma = 0.95$ or $\tau \approx 6$ for $\gamma = 0.7$) reflect transient phase reversals in the corresponding impulse response that result from beating between contributions from the two poles in the admittance near $f \approx f_{CF}$ (cf. Fig. 3). Note how the fine time structure for all three responses (i.e., pressure, admittance, and velocity) remains approximately independent of γ (i.e., of intensity). Indeed, the corresponding IF trajectories can be difficult to distinguish in the plot; their asymptotic values generally differ by less than 5% over the entire range of γ.

How do the poles move with intensity? As γ decreases from 1, the double pole splits apart, and the poles move out along the solid lines in the directions shown by the arrows. The symbols ($\times$) mark off equal intervals of γ along each trajectory. As γ approaches 0, all but one of the poles (and its counterpart in the negative-frequency half-plane) move off towards infinity. In the limit $\gamma \to 0$, the mechanical admittance $Y_{BM}(\zeta;\gamma)$ takes the form of a passive harmonic oscillator (Y_p) characterized by a single pole near $\zeta = 1.03 + 0.17i$. Recall from Sec. III B that the parameters of the oscillator $Y_p(\beta)$ characterizing the passive system at high sound levels ($\gamma = 0$) were chosen so that its single pole would lie almost directly above the double pole characterizing the combined (i.e., ''active+passive'') system at low levels ($\gamma = 1$). In other words, the natural ''resonant frequencies'' of the two systems, given by the real parts of the pole locations, are nearly identical. As a consequence of the approximate alignment of pole locations at the two extremes ($\gamma = 1$ and $\gamma = 0$)—and the corresponding invariance of natural resonant frequencies—the poles at intermediate values of γ also remain fairly close to the line $\mathrm{Re}\{\zeta\} = 1.03$. Although the poles separate slightly, they do so almost symmetrically about the line $\mathrm{Re}\{\zeta\} = 1.03$, so that their mean frequency stays nearly constant.

3. Impulse responses

If our conjecture is correct, we expect the fine time structure of the model impulse responses to be approximately independent of intensity (since the poles of the admittance are confined to a relatively narrow strip of the complex plane). Figure 4 demonstrates that model $\mathcal{M}^{\approx}$ does indeed capture this symmetry of the data. The figure shows model pressure, admittance,[15] and velocity impulse responses, along with corresponding instantaneous-frequency (IF) trajectories, computed at several values of γ. As discussed above, the responses at different γ can be interpreted as derived impulse responses (input–output cross-correlation functions) obtained from a single nonlinear model at different intensities (and subsequently normalized by the input at the stapes). As γ decreases (i.e., as intensity increases), the response envelopes shrink in size (the nonlinearity is compressive) and peak at progressively earlier times. Note, however, that despite these changes in the envelope of the response, the fine time structure remains almost independent of γ. For example, the asymptotic values of the IF trajectories differ by less than 5% over the entire range of γ. Frequency-domain analogues of these intensity effects—namely a strong reduction in peak amplitude accompanied by relatively small but systematic changes in phase below CF (e.g., Rhode and Recio, 2000)—can be seen in the model BM velocity transfer functions $T(\beta;\gamma)$ shown in Fig. 2.

D. Other models of intensity dependence

In model $\mathcal{M}^{\approx}$ described above the approximate invariance with intensity of the fine time structure of the impulse response is a direct consequence of the roughly vertical alignment of admittance-pole locations about the line $\mathrm{Re}\{\zeta\} = 1.03$. We illustrate this point by considering two other heuristic models of the intensity dependence of the BM admittance.

1. Model $\mathcal{M}^{<}$

In model $\mathcal{M}^{<}$, the resonant frequency of the passive admittance $Y_p(\beta)$ obtained in the limit $\gamma \to 0$ is taken to be roughly one-half octave below CF [i.e., $\nu = f_p(x)/f_{CF}(x) \approx \sqrt{2}/2$]. As a consequence of this half-octave downwards shift in resonant frequency, the admittance-pole trajectories are no longer confined to the vicinity of the line $\mathrm{Re}\{\zeta\} = 1.03$. As illustrated in Fig. 5(b), the pole closest to the real axis moves off to lower frequencies as γ decreases; at $\gamma = 0$, the pole converges on the passive pole at $\zeta \approx 0.77 + 0.17i$. Figure 6(a) shows that this variation in resonant frequency destroys the near-invariance of fine time structure (cf. model $\mathcal{M}^{\approx}$ in Fig. 4). As expected, the asymptotic frequencies of corresponding IF trajectories (not shown) vary systematically with γ, decreasing by roughly half an octave as γ approaches 0. In

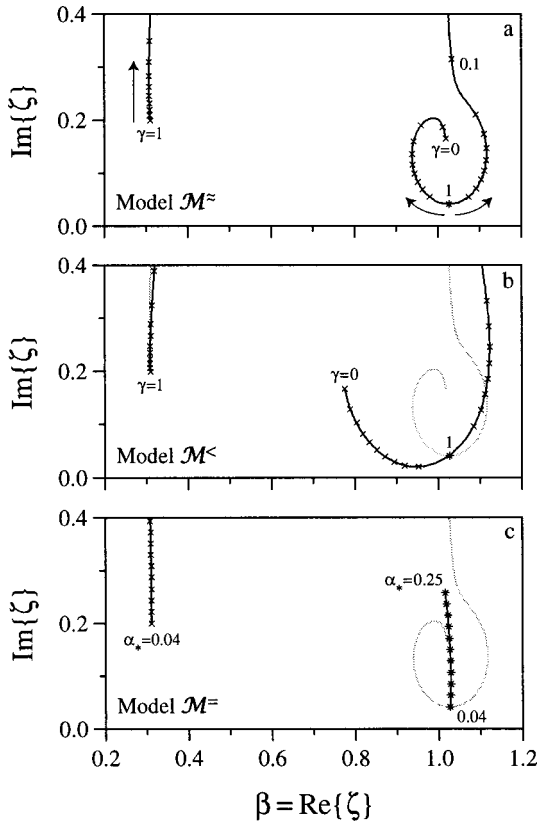

FIG. 5. Admittance-pole trajectories in the complex plane. The three panels [(a), (b), and (c)] show trajectories in the ζ plane of the principal positive-frequency poles of the BM admittance for three different model forms ($\mathcal{M}^{\approx}$, $\mathcal{M}^{<}$, and $\mathcal{M}^{=}$) of the intensity dependence. Panel (a), reproduced from Fig. 3, shows the pole trajectories for model $\mathcal{M}^{\approx}$ as a function of γ. At $\gamma=1$, $Y_{\mathrm{BM}}(\zeta;\gamma)$ has a double pole (*) at $\zeta_*=1.03+i0.04$. As γ decreases the two poles separate slightly and move out along the solid lines in the directions shown by the arrows. Markers (×) measure off ten equal intervals of γ spanning the range 0–1. In the limit $\gamma\to 0$, all but one of the poles move off towards infinity, and the admittance $Y_{\mathrm{BM}}(\zeta;\gamma)$ becomes a passive harmonic oscillator, $Y_{\mathrm{p}}(\zeta)$. Panel (b) shows the pole trajectories for model $\mathcal{M}^{<}$ as a function of γ. As in panel (a), markers (×) measure off ten equal intervals of γ spanning the range 0–1. In model $\mathcal{M}^{<}$, the resonant frequency of the passive admittance $Y_{\mathrm{p}}(\beta)$ obtained in the limit $\gamma\to 0$ is roughly one-half octave below CF. For comparison, the gray lines show the trajectories from model $\mathcal{M}^{\approx}$. Panel (c) shows the pole trajectories for model $\mathcal{M}^{=}$ as a function of α_*, the imaginary part of the double pole of the admittance. Markers (×) measure off ten equal intervals of α_* spanning the range 0.04–0.25. In model $\mathcal{M}^{=}$, the double poles of the admittance $Y_{\mathrm{BM}}(\zeta;\alpha_*)$ move along a curve nearly perpendicular to the real frequency axis. Note that all three models are identical in the low-level linear limit (i.e., for $\gamma=1$ in models $\mathcal{M}^{\approx}$ and $\mathcal{M}^{<}$ and for $\alpha_*=0.04$ in model $\mathcal{M}^{=}$).

the frequency domain, the model BM transfer functions [see Fig. 7(b)] manifest unrealistically large shifts in peak frequency as well as considerable changes in phase below CF.

2. Model $\mathcal{M}^{=}$

Our analysis predicts exact invariance of fine time structure when the poles of the admittance move along vertical lines. The pole trajectories of model $\mathcal{M}^{=}$, illustrated in Fig. 5(c), approximate this ideal, limiting case. To achieve near-perfect alignment of the pole positions in model $\mathcal{M}^{=}$, we began, as before, with the double-pole form of the BM admittance described in Sec. III A. But rather than simulating intensity dependence by varying γ in the two-component form of the impedance, as we did in models $\mathcal{M}^{\approx}$ and $\mathcal{M}^{<}$, we varied the imaginary part of the double pole directly (see Note 8). By varying the imaginary part of the double pole (denoted $\alpha_*\equiv\mathrm{Im}\{\zeta_*\}$, where the subscripted asterisk symbolizes a double pole), we constrain the principal poles of the model admittance, $Y_{\mathrm{BM}}(\zeta;\alpha_*)$, to move along a nearly vertical line in the complex plane (i.e., along a line $\beta_*\approx$constant).[16] As a consequence of this difference in model structure, the model $\mathcal{M}^{=}$ impedances, $Z_{\mathrm{BM}}(\beta;\alpha_*)$, are only approximately of the two-component form given by Eq. (5). Figure 6(b) shows that near-vertical alignment of admittance pole locations yields near-perfect invariance of fine time structure. The corresponding frequency-domain transfer functions [see Fig. 7(c)] are, on this scale, almost indistinguishable from those of model $\mathcal{M}^{\approx}$.

E. Recapitulation

Figure 8 summarizes the intensity dependence of the fine time structure in each of the three models (see also Table I). Models $\mathcal{M}^{\approx}$ and $\mathcal{M}^{=}$ manifest the near-invariance of fine time structure seen in measured responses, and in these models the poles of the BM admittance move along trajectories roughly perpendicular to the real frequency axis. We suggest that this result applies to the real cochlea: The approximate invariance of the fine time structure of the impulse response implies that the poles of the effective BM admittance remain within relatively narrow bands of the complex plane oriented perpendicular to the real frequency axis as the stimulus intensity is varied. We expect our conjecture to apply so long as the driving pressure force $p(\tau;\gamma)$ inherits its intensity dependence through the admittance, as it does in simple models. Physically, our conjecture implies that the natural resonant frequencies of the cochlear partition are nearly independent of intensity. Put yet another way, the feedback forces generated by the outer hair cells (or, more generally, by the ''cochlear amplifier'') do not significantly change the natural resonant frequencies of the cochlear partition.

IV. CONSISTENCY WITH THE ''HALF-OCTAVE SHIFT''

Is our conjecture that the resonant frequencies of the cochlear partition are nearly independent of intensity contradicted by the well-known intensity dependence of the peak (or best) frequency of the BM transfer function, which shifts to lower frequencies at higher intensities? Reference to the responses of models $\mathcal{M}^{\approx}$ and $\mathcal{M}^{=}$ in Fig. 7 demonstrates that the answer is ''No.'' Note, for example, that although the poles of the model-$\mathcal{M}^{=}$ admittance move nearly vertically—and the resonant frequencies are therefore essentially independent of intensity—the best frequency (BF) of the transfer function shifts systematically with level from a peak at $f/f_{\mathrm{CF}}=1$ (for $\alpha_*=0.04$) to a peak roughly one-half octave lower (at $\alpha_*=0.25$). Models $\mathcal{M}^{\approx}$ and $\mathcal{M}^{=}$ therefore reproduce the ''half-octave shift'' in best frequency without any corresponding change in the underlying resonant frequencies of the system.

If the half-octave shift does not reflect a change in the local resonant frequency of the cochlear partition (e.g., due to a change in stiffness), what then is the mechanism that

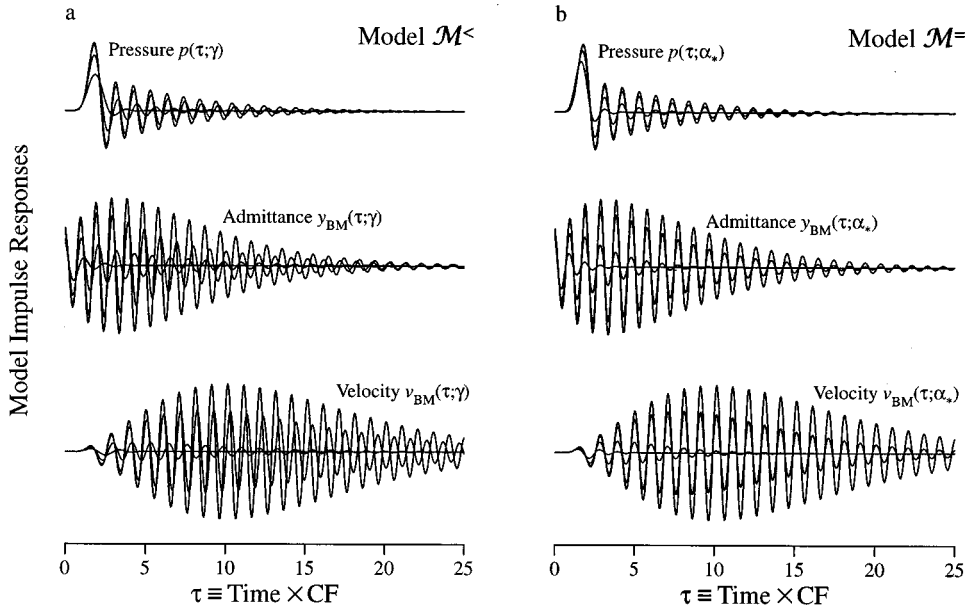

FIG. 6. Impulse responses for two different model forms ($\mathcal{M}^<$ and $\mathcal{M}^=$) of the intensity dependence of the effective BM admittance. Panel (a) shows model $\mathcal{M}^<$ impulse responses for several values of γ. As in Fig. 4, the figure shows impulse responses for model pressure, admittance, and velocity responses (top to bottom, respectively). Responses are computed for $\gamma=\{1,0.95,0.7,0\}$ and are normalized by input at the stapes so that response amplitudes decrease at smaller values of γ (i.e., at higher intensities). In model $\mathcal{M}^<$, the resonant frequency of the passive admittance $Y_p(\beta)$ obtained in the limit $\gamma\rightarrow 0$ is roughly one-half octave below CF. Note how the fine time structure of the response varies strongly with γ (i.e., with intensity). Panel (b) shows model $\mathcal{M}^=$ impulse responses for several values of α_*. Responses are computed for $\alpha_*=\{0.04,0.05,0.1,0.25\}$ and normalized by input at the stapes so that response amplitudes decrease at larger values of α_* (i.e., at higher intensities). In model $\mathcal{M}^=$, the double poles of the admittance $Y_{BM}(\zeta;\alpha_*)$ move along a curve nearly perpendicular to the real frequency axis. As a result, the fine time structure is essentially independent of intensity.

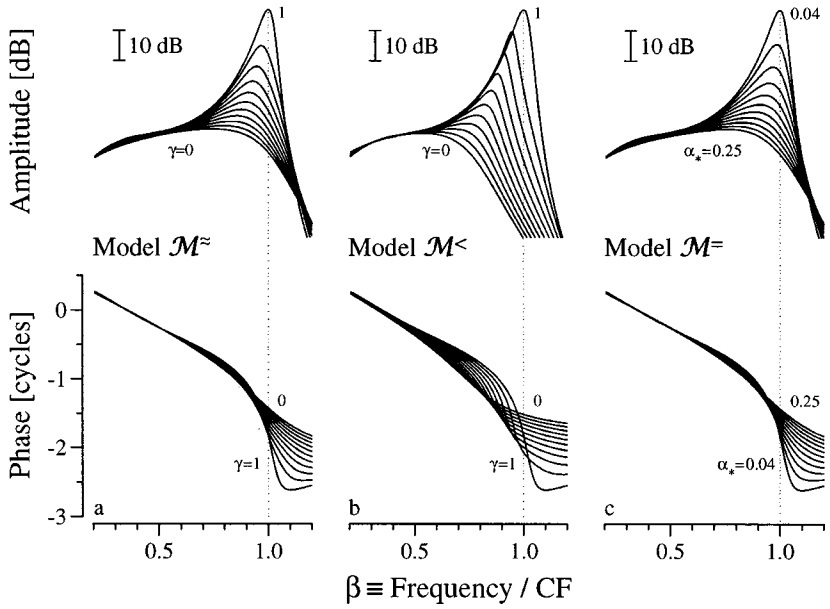

FIG. 7. Intensity dependence of model BM velocity transfer functions. The three panels [(a), (b), and (c)] show the amplitude (top) and phase (bottom) of the BM velocity transfer function (BM/stapes) for three different model forms ($\mathcal{M}^\approx$, $\mathcal{M}^<$, and $\mathcal{M}^=$) of the intensity dependence of the BM admittance. Panel (a) shows transfer functions for model $\mathcal{M}^\approx$, defined by the admittance-pole trajectories in Fig. 5(a). Reproduced from Fig. 2, the model-$\mathcal{M}^\approx$ transfer functions are shown for values of γ corresponding to the markers ($\times$) in Fig. 5(a) (i.e., for eleven values spanning the range 0–1 in steps of 0.1). In model $\mathcal{M}^\approx$, the resonant frequency of the passive admittance $Y_p(\beta)$ is equal to CF. Panel (b) shows transfer functions for model $\mathcal{M}^<$ at the values of γ given by the markers on the admittance-pole trajectories of Fig. 5(b). In model $\mathcal{M}^<$, the resonant frequency of the passive admittance Y_p is roughly one-half octave below CF. Panel (c) shows transfer functions for model $\mathcal{M}^=$ at the values of α_* given by the markers on the admittance-pole trajectories of Fig. 5(c). In model $\mathcal{M}^=$, the double poles of the admittance $Y_{BM}(\zeta;\alpha_*)$ move along a curve nearly perpendicular to the real frequency axis. Note that all three models are identical in the low-level linear limit.

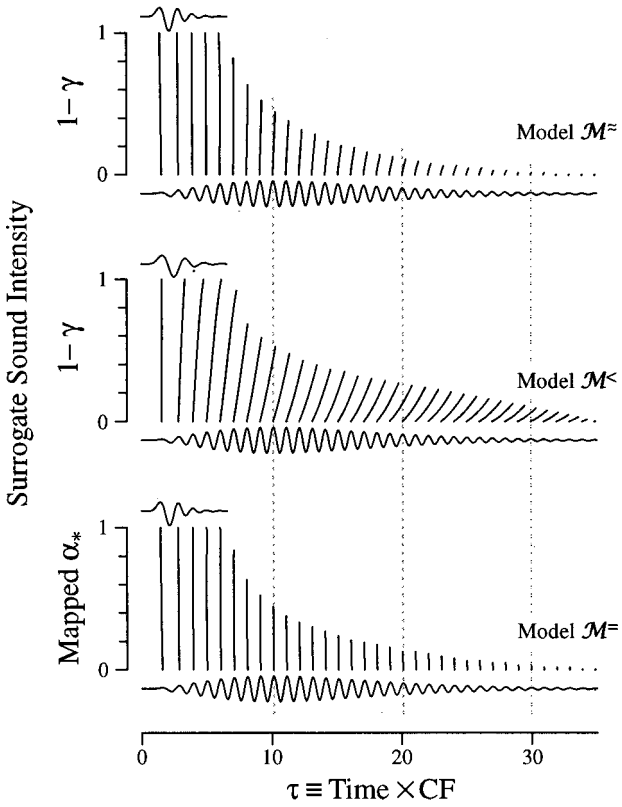

FIG. 8. Variation of fine time structure in impulse responses for three different model forms ($\mathcal{M}^{\approx}$, $\mathcal{M}^{<}$, and $\mathcal{M}^{=}$) of the intensity dependence of the effective BM admittance. In the top panel, the nearly vertical lines represent trajectories, traced out as the parameter γ is varied over the interval [0,1], marking the times of occurrence of corresponding peaks in the model-$\mathcal{M}^{\approx}$ BM velocity impulse response. So that intensity increases from top to bottom along the axis, the surrogate value $1-\gamma$ is shown along the ordinate. Time is plotted along the abscissa in units of periods of CF. Normalized response waveforms, corresponding to $\gamma=0$ and $\gamma=1$, respectively, appear at the top and bottom of each panel. At each surrogate intensity, trajectories are plotted over a total time interval equal to three times the energy-weighted average group delay of the response (truncated to the nearest whole period). The middle panel shows trajectories for model $\mathcal{M}^{<}$ in the same format as the top panel. The bottom panel shows trajectories for model $\mathcal{M}^{=}$. The ordinate shows values of α_* in the range [0.04,0.25] remapped linearly onto the interval [0,1], using the equation $\hat{\alpha}_*=[\alpha_* - \min(\alpha_*)]/[\max(\alpha_*) - \min(\alpha_*)]$, for consistency in the display. The three vertical dotted lines spanning the figure mark selected peaks in the model-$\mathcal{M}^{=}$ waveform.

creates the shift in best frequency? The answer—as with the origin of the glide (Shera, 2001)—is to be found not in the admittance, but in the driving pressure; not locally at the point of measurement, but globally in the spatial variation of geometry and mechanics that underlies the cochlear map. To see this, consider model $\mathcal{M}^{\approx}$ and recall that the BM velocity impulse response, $v_{\mathrm{BM}}(\tau;\gamma)$, is the convolution of $p(\tau;\gamma)$ and $y_{\mathrm{BM}}(\tau;\gamma)$ [Eq. (3)]. Although the best frequency of the admittance spectrum is nearly independent of intensity, the same is not true of the pressure. As intensity increases, the amplification of the traveling pressure wave is reduced. As a consequence, the pressure impulse response $p(\tau;\gamma)$ decays from its maximum amplitude more quickly and its ''center of energy'' moves to earlier times (see Fig. 4). Because of traveling-wave dispersion (Shera, 2001), however, $p(\tau;\gamma)$ at early times is dominated by the glide, which, in the base of the cochlea, consists primarily of frequencies below CF. Thus, as the duration of the driving pressure $p(\tau;\gamma)$ shortens with increasing intensity, the period of the glide becomes an ever-increasing fraction of the total duration of the response. As a result, the motion of the membrane at the measurement location becomes more and more dominated by driving frequencies lower than CF. The peak of the velocity spectrum (i.e., the best frequency) therefore shifts to lower frequencies.[17] Thus, as with the glide (Shera, 2001), the shift in BF arises not through the *local* properties of the cochlear partition—the resonant frequencies of Y_{BM} change neither with time nor with intensity—but through the *global* properties of the driving pressure.

TABLE I. Summary of the three different model forms of the intensity dependence of the effective BM admittance discussed in this paper.

Summary of models			
Model	Description	Formula	Invariance?
$\mathcal{M}^{\approx}$	Resonant frequency of Y_{p} approximately equal to CF	$f_{\mathrm{p}}(x)\approx f_{\mathrm{CF}}(x)$	Very good
$\mathcal{M}^{<}$	Resonant frequency of Y_{p} approximately one-half octave below CF	$f_{\mathrm{p}}(x)\approx f_{\mathrm{CF}}(x)/\sqrt{2}$	Poor
$\mathcal{M}^{=}$	Poles of the BM admittance move along lines nearly perpendicular to the real frequency axis	$\beta_*\approx$ constant	Excellent

A. Complementary shifts in best frequency and bandwidth

In addition to the half-octave shift, models $\mathcal{M}^{\approx}$ and $\mathcal{M}^{=}$ capture another important characteristic of the intensity dependence of BM transfer functions. As illustrated in Fig. 7, the best frequency changes relatively little over the first 30 dB reduction in peak amplitude; the bulk of the frequency shift occurs at the highest intensities over a relatively small

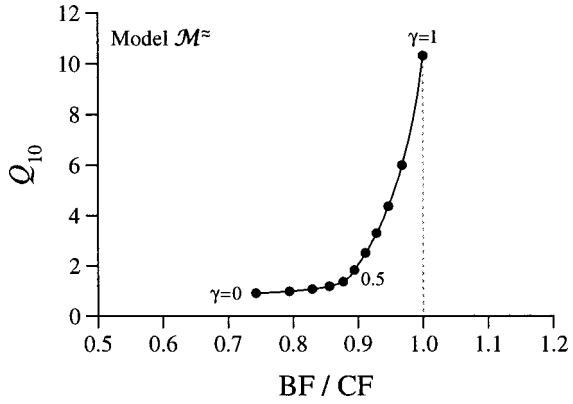

FIG. 9. Intensity dependence of transfer-function bandwidth and best frequency in model $\mathcal{M}^{\approx}$. The figure plots the Q_{10} vs the normalized best frequency (BF/CF) of the model transfer-function $T(\beta;\gamma)$ with γ as parameter. Q_{10} is defined as the ratio $\mathrm{BF}/\Delta f_{10}$, where Δf_{10} is the transfer-function bandwidth 10 dB below the peak. The dots mark the eleven values of γ corresponding to the markers on the admittance-pole trajectories in Fig. 3; they span the range 0–1 in steps of 0.1. The dotted line marks the value BF/CF=1 obtained in the low-level linear limit near threshold. Note that changes in BF and Q_{10} occur over complementary intensity ranges: Most of the change in BF occurs for $0\lesssim\gamma\lesssim 0.5$; most of the change in Q_{10} for $0.5\lesssim\gamma\lesssim 1$.

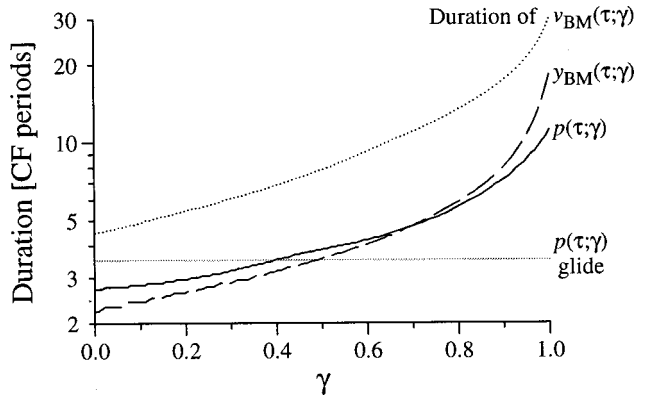

FIG. 10. Impulse-response durations in model $\mathcal{M}^{\approx}$. The figure shows the durations of the impulse responses $p(\tau;\gamma)$ (solid line), $y_{BM}(\tau;\gamma)$ (dashed line), and $v_{BM}(\tau;\gamma)$ (dotted line) as a function of γ. Response duration is defined here as the time (in periods of the CF) at which the envelope of the response decays to 10% of its peak value. As expected from the convolution in Eq. (2), the duration of $v_{BM}(\tau;\gamma)$ is approximately equal to the sum of the durations of $p(\tau;\gamma)$ and $y_{BM}(\tau;\gamma)$. The gray line shows the duration of the glide in the pressure $p(\tau,\gamma)$, defined as the time at which the instantaneous frequency reaches 90% of CF. Its value is independent of γ. Note that the durations of $p(\tau;\gamma)$ and $y_{BM}(\tau;\gamma)$ become comparable to the duration of the pressure glide at $\gamma\approx 0.5$, corresponding roughly with the value of γ at the bend in the curve of Fig. 9.

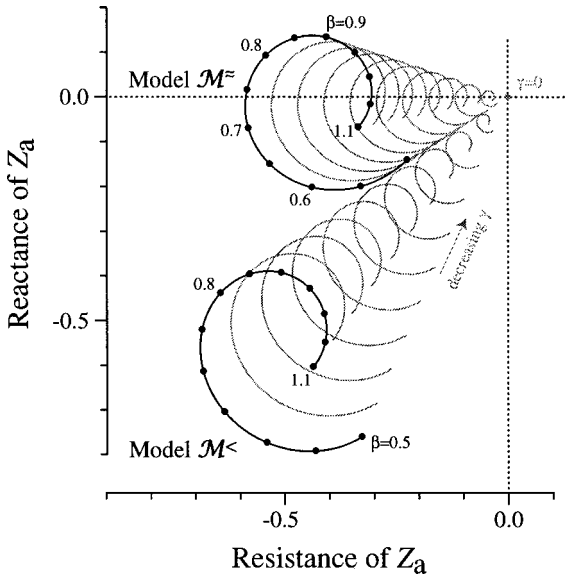

FIG. 11. Polar plot of the impedance $Z_a(\beta)$ for models $\mathcal{M}^{\approx}$ and $\mathcal{M}^{<}$. The two black curves trace out the real (resistive) and imaginary (reactive) parts of $Z_a(\beta)$ as β varies over the interval [0.5,1.1] containing the peak of the transfer function. Dots on the two curves indicate equal intervals (0.05) of β. The gray lines show how the effective impedance $\gamma Z_a(\beta)$ changes as γ decreases to 0 in steps of 0.1. Dotted lines mark the positions of the real and imaginary axes.

part of the total dynamic range. The curve shown in Fig. 9 quantifies this nonuniform shift in BF for model $\mathcal{M}^{\approx}$. Figure 9 also illustrates how changes in the best frequency and bandwidth of the response occur over complementary parts of the intensity range, in agreement with experimental data (e.g., Møller, 1977). Note, in addition, that the slope of the curve indicates that the bandwidth of the transfer function is a strong function of γ at values of γ close to 1. Even small reductions in the effective strength of the cochlear amplifier (e.g., due to surgical trauma) can therefore produce relatively large changes in the bandwidth (and group delay) of the response to threshold-level sounds.

The nonuniform shift in best frequency with intensity can be understood from the conceptual model used to explain the half-octave shift. The model suggests that shifts in the BF of $v_{BM}(\tau;\gamma)$ remain relatively small so long as the impulse responses $p(\tau;\gamma)$ and $y_{BM}(\tau;\gamma)$ last longer than the duration of the pressure glide. Figure 10 compares these durations as a function of γ for model $\mathcal{M}^{\approx}$. Although quantitative details depend on precisely how one defines the duration of the response, model results are qualitatively consistent with the conceptual analysis. At values $\gamma\gtrsim 0.5$, both $p(\tau;\gamma)$ and $y_{BM}(\tau;\gamma)$ last longer than the duration of the glide, and the BF therefore changes relatively little with intensity (cf. Fig. 9). At values $\gamma\lesssim 0.5$, however, the durations of both $p(\tau;\gamma)$ and $y_{BM}(\tau;\gamma)$ become comparable to or less than the length of the glide, and intensity-related shifts in BF become larger.

V. CONSTRAINTS ON THE MECHANISMS OF COCHLEAR AMPLIFICATION

In Sec. III B we represented the total basilar-membrane impedance $Z_{BM}(\beta;\gamma)$ in the form

$$Z_{BM}(\beta;\gamma)=Z_p(\beta)+\gamma Z_a(\beta), \tag{10}$$

representing the sum of a passive and an active component (Z_p and Z_a, respectively), where the coefficient of Z_a varies with intensity. For purposes of explication we have regarded the two models $\mathcal{M}^{\approx}$ and $\mathcal{M}^{<}$—which are, by construction, identical in the low-level linear limit ($\gamma=1$)—as differing in the form of the underlying passive impedances, Z_p. In particular, the passive impedances in these two models were taken to differ in the locations of their resonant frequencies relative to CF. To explore the implications of our results for cochlear biophysics, we now take a complementary view and ask: What constraint does the intensity-invariance of BM resonant frequencies place on the mechanical effects of force generation by outer hair cells, as characterized by the active impedance Z_a?[18]

A. Two-component form of $Z_a(\beta)$

We begin by examining the form of $Z_a(\beta)$ in models $\mathcal{M}^{\approx}$ and $\mathcal{M}^{<}$. For impedances of the two-component form (10), the active impedance $Z_a(\beta)$ can be obtained by simple subtraction of the impedances $Z_{BM}(\beta)$ and $Z_p(\beta)$ characterizing the low- and high-level linear limits, respectively: $Z_a(\beta)=Z_{BM}(\beta)-Z_p(\beta)$. Figure 11 shows a polar plot of the impedance $Z_a(\beta)$ for the models $\mathcal{M}^{\approx}$ and $\mathcal{M}^{<}$. For reference, Fig. 12 shows corresponding values of $Z_{BM}(\beta;\gamma)$ and their variations with γ. The solid curves in Fig. 11 trace out the real and imaginary parts of the model impedances $Z_a(\beta)$ as β varies over the interval [0.5,1.1] containing the peak of the transfer function. We focus on this region because outside the peak region the BM impedance obtained by solution of the inverse problem is less reliable (and its precise form less important in determining the shape of the transfer function).

In both models, $Z_a(\beta)$ resembles a spiral arc, offset

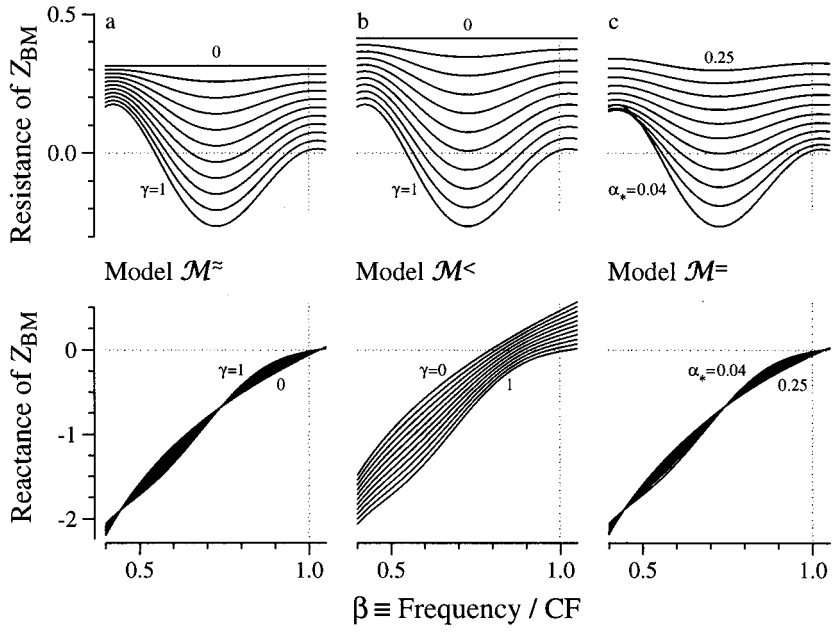

FIG. 12. Intensity dependence of model BM impedance functions. The three panels [(a), (b), and (c)] show the real (top) and imaginary parts (bottom) of $Z_{BM}(\beta;\gamma)$ for the three different model forms ($\mathcal{M}^{\approx}$, $\mathcal{M}^{<}$, and $\mathcal{M}^{=}$) of its intensity dependence defined by the admittance-pole trajectories in Fig. 5. Panel (a) shows impedances for model $\mathcal{M}^{\approx}$, reproduced from Fig. 2, at values of γ corresponding to the markers ($\times$) in Fig. 5(a). Panel (b) shows impedances for model $\mathcal{M}^{<}$ at the values of γ corresponding to the markers in Fig. 5(b). Panel (c) shows impedances for model $\mathcal{M}^{=}$ at the values of α_* corresponding to the markers in Fig. 5(c). Units are defined so that the proportionality constant in Eq. (9) for $Y_{BM}(\beta)$ equals unity. The impedances of all three models are identical in the low-level linear limit.

from the origin and traced out clockwise at nearly constant ''angular velocity'' as β increases uniformly. As γ decreases from 1, the spiral arcs contract towards the origin. Figure 11 suggests that the impedance $Z_a(\beta)$ can be approximated as the sum of two components:[19]

$$Z_a(\beta) \approx Z_a^{\text{constant}} + Z_a^{\text{spiral}}(\beta), \tag{11}$$

where Z_a^{constant} is a frequency-independent component that locates the center of the spiral and $Z_a^{\text{spiral}}(\beta)$ traces out the spiral by circling about Z_a^{constant}. The two models $\mathcal{M}^{\approx}$ and $\mathcal{M}^{<}$ differ primarily in the form of Z_a^{constant}. In model $\mathcal{M}^{\approx}$, the impedance Z_a^{constant} is negative real (a negative resistance). In model $\mathcal{M}^{<}$, however, Z_a^{constant} is complex, implying that it affects both the resistance and the reactance of the partition. These impedance changes, and their dependence on γ, are evident in the plots of $Z_{BM}(\beta;\gamma)$ shown in Fig. 12.

The constant impedance change effected by Z_a^{constant} is modulated with frequency by $Z_a^{\text{spiral}}(\beta)$, and these modulations appear in $Z_{BM}(\beta;\gamma)$. For example, the real part of $Z_{BM}(\beta;\gamma)$ manifests a bowl-shaped minimum centered roughly one-half octave below CF (see Fig. 12). The depth of the bowl, but not its ''axis of symmetry,'' varies with γ, reaching its furthest negative excursion at $\gamma=1$ (i.e., at low intensities). As discussed in Sec. III C, these variations with intensity are similar to those seen in impedances estimated using the inverse method (de Boer and Nuttal, 2000).

The bowl-shaped form of $\text{Re}\{Z_{BM}(\beta;\gamma)\}$ evident in both models is created by the oscillation in $\text{Re}\{Z_a^{\text{spiral}}(\beta)\}$, which reaches a minimum near $\beta\approx 0.74$ corresponding to the bottom of the bowl. The impedance $Z_a^{\text{spiral}}(\beta)$ also modulates the reactance, creating frequency oscillations in $\text{Im}\{Z_{BM}(\beta;\gamma)\}$ that appear roughly 90° out of phase with the modulations in the resistance. As discussed below in Sec. V B, oscillations in the resistance and reactance that appear 90° out of phase with one another are expected from causality, which requires that the real and imaginary parts of $Z_a(\beta)$ be Hilbert transforms of one another. In both models $\text{Im}\{Z_a^{\text{spiral}}(\beta)\}$ increases the effective stiffness of the partition in parts of the ''tail'' of the transfer function ($\beta \lesssim 0.74$) while decreasing the stiffness throughout most of the peak region ($0.74 \lesssim \beta \lesssim 1.03$).

Significantly, $\text{Im}\{Z_a^{\text{spiral}}(\beta)\}$ passes through 0, so that $Z_a^{\text{spiral}}(\beta)$ is nearly real, just above CF at $\beta\approx 1.03$. In model $\mathcal{M}^{\approx}$, where Z_a^{constant} is also nearly real, the zero crossing of $\text{Im}\{Z_a^{\text{spiral}}(\beta)\}$ implies that the impedance $Z_a(\beta)$ leaves the reactive component of the total partition impedance near this value of β essentially unchanged at all intensities. Reference to Fig. 12(a) shows that in model $\mathcal{M}^{\approx}$ the value $\beta\approx 1.03$ is the value where the reactive component of $Z_p(\beta)$ vanishes. Since $\text{Im}\{Z_p(\beta)\}$ and $\text{Im}\{Z_a(\beta)\}$ both vanish at the same value of β, their sum, $\text{Im}\{Z_{BM}(\beta;\gamma)\} = \text{Im}\{Z_p(\beta)\} + \gamma\text{Im}\{Z_a(\beta)\}$, also vanishes at this point and does so independent of γ. Note, however, that the vanishing of the reactance [zero crossing of $\text{Im}\{Z_{BM}(\beta;\gamma)\}$] locates the approximate natural resonant frequency of the partition [i.e., the projection of the nearby pole of the admittance $Y_{BM}(\beta;\gamma)$ along the real frequency axis].[20] Our analysis of the impedance $Z_a(\beta)$ has therefore brought us full circle: In model $\mathcal{M}^{\approx}$ we conclude that the natural resonant frequencies of the partition must be nearly independent of intensity. In model $\mathcal{M}^{<}$, by contrast, Z_a^{constant} is large and complex so that $\text{Im}\{Z_a(\beta)\}$ is always negative; in this model, therefore, $Z_a(\beta)$ modifies the reactive component of the impedance at all frequencies and intensities [see Fig. 12(b)]. As a consequence, the resonant frequencies of the partition depend on γ.

Our analysis has thus identified the constraint that intensity invariance of the resonant frequencies places on the mechanical effect of force generation by OHCs, as summarized in the impedance $Z_a(\beta)$: While generally affecting a substantial reduction in the effective damping, the OHCs must not significantly change the reactance of the passive partition at frequencies in a neighborhood about its natural resonant frequency.[21]

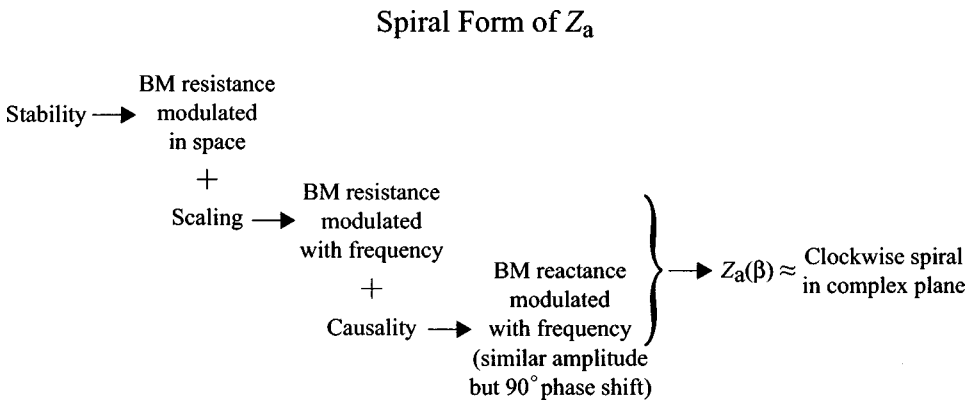

FIG. 13. Summary of the argument deducing the qualitative form of $Z_a(\beta)$ from general physical principles (stability, local scaling, and causality). The argument implies that $Z_a(\beta)$ has an approximately spiral form in the complex plane. The near-invariance of the fine time structure in the impulse response locates this spiral near the real (i.e., resistive) axis.

B. General argument for the spiral form of $Z_a(\beta)$

Illustrated above for two specific models (i.e., $\mathcal{M}^{\approx}$ and $\mathcal{M}^{<}$), the approximately spiral form of the impedance $Z_a(\beta)$ can be deduced from general principles. Figure 13 summarizes the argument. For the cochlea to remain stable, the damping of the partition cannot everywhere be negative. Stability requires that energy added to the traveling wave in one region be absorbed in another; the amplifier must therefore create negative damping over only a finite region of the cochlea (e.g., just basal to the peak of the traveling wave). Thus, the effective damping must be modulated in space. According to local scaling symmetry, however, modulation in space (at fixed frequency) requires a corresponding modulation in frequency (at fixed position). But in the frequency domain, causality implies that the real and imaginary parts of an impedance are not independent; rather, they are Hilbert transforms of one another (e.g., Bode, 1945; Papoulis, 1977). Thus, frequency modulations in the damping (real part) are necessarily accompanied by frequency modulations of similar amplitude in the reactance (imaginary part).[22] Since the Hilbert transformer acts like a 90° phase shifter (e.g., the Hilbert transform of a cosine modulation is a $-$sine), the frequency modulations (oscillations) in the damping and reactance are roughly 90° out of phase with one another. In Fig. 12(a), for example, regions of local decrease in the damping (e.g., near $\beta \approx 0.6$) correspond to local minima in the reactance oscillation, local minima in the damping (e.g., the bottom of the bowl near $\beta \approx 0.74$) correspond to regions of local increase in the reactance, and so on. As a consequence of these coupled modulations in resistance and reactance, $Z_a(\beta)$ must have an approximately spiral form traced out clockwise with increasing β (cf. Fig. 11).

This general argument yields only the approximate *shape* of the $Z_a(\beta)$ trajectory in the complex plane; it does not, of course, determine the radius of the spiral, the way the radius changes with β, nor the rate at which the spiral is traversed. Neither does the argument locate the absolute position of the spiral (i.e., the value of Z_a^{constant}) in the complex plane. As illustrated above in Sec. V A, the location of the spiral—straddling the real-frequency axis—is set by the requirement of near-invariance of fine time structure. If the resonant frequencies of the partition are to remain invariant, the impedance $Z_a(\beta)$ must leave the partition reactance unchanged at frequencies near CF.

Guided by simple models based on the inverse solution in the low-level linear regime (Zweig, 1991), we have used general principles (stability, local scaling, and causality) and the intensity-invariance of the fine time structure of the impulse response to deduce the qualitative form of $Z_a(\beta)$ representing the collective action of the OHCs. At frequencies about CF, the impedance $Z_a(\beta)$ must (1) be roughly spiral in form, (2) rotate clockwise with increasing frequency about a center with a negative real part, and (3) intersect (or at least approach) the real (resistive) axis near the natural resonant frequency of the passive partition.

C. Implications for the origin of negative damping: The fast-time-delayed stiffness model

Among the most biophysically plausible models so far proposed for the origin of negative damping has been the fast-time-delayed stiffness model (Neely, 1983; Zweig, 1990, 1991). This model is based on the observation that a negatively damped oscillator can be created from one with positive damping by the addition of a feedback force proportional to the oscillator's displacement at a previous time (i.e., a time-delayed stiffness). The impedance of a time-delayed stiffness can be written in the form

$$Z_f = \frac{K_f}{i\omega} e^{-i\omega\tau_f}, \tag{12}$$

where $K_f > 0$ is the amplitude and $\tau_f > 0$ the time delay of the feedback force. Represented in vector form, a pure stiffness (such as $K_f/i\omega$) points along the negative imaginary axis. The time delay has the effect of rotating this stiffness vector clockwise through the angle $\omega\tau_f$. For $0 < \omega\tau_f < \pi$ the time delay rotates the impedance vector into the negative real half plane, giving the impedance Z_f a negative real part. In this configuration, the feedback force can therefore reduce the damping of the system to which it is coupled.

An attractive feature of the model is that when the time delay is small compared to the period of the driving frequency, so that

$$0 < |\omega\tau_f| \ll 1, \tag{13}$$

the resistive component of Z_f is negative over a wide range of frequencies (specifically, for all $f < 1/2\tau_f$). Thus, if the feedback force is sufficiently strong and delayed by a nonzero time small compared to the oscillator's period, it can create negative damping over a broad range of characteristic

frequencies without recourse to additional tuning mechanisms (such as having the time delay vary strongly with position in the cochlea). Transduction delays on the order of a few microseconds have been suggested (Neely, 1983; Zweig, 1990); we therefore follow Zweig and label the impedance Z_f and its parameters with the subscript ''f'' for ''fast.'' Note, however, that in addition to reducing the resistance, Z_f also generally changes the reactive component of the system (e.g., its stiffness). Of course, whether Z_f produces a significant change in *either* the net resistance or reactance depends on the system to which the impedance is coupled. In the paragraphs that follow we argue that in the context of cochlear mechanics (as currently understood) the fast-time-delayed stiffness model cannot provide sufficient force to counteract the damping without also producing significant effects on the stiffness.

Zweig (1991) analyzed the fast-time-delayed stiffness model in detail; we begin by recapitulating key elements of that analysis. When the time delay is sufficiently fast to satisfy Eq. (13), the complex exponential in Eq. (12) can be expanded in powers of its argument:

$$e^{-i\omega\tau_f} = 1 - i\omega\tau_f - \tfrac{1}{2}\omega^2\tau_f^2 + \ldots . \tag{14}$$

Keeping the first three terms yields

$$Z_f = K_f/i\omega + R_f + i\omega M_f, \tag{15}$$

where

$$R_f \equiv -K_f\tau_f \quad \text{and} \quad M_f \equiv \tfrac{1}{2}K_f\tau_f^2. \tag{16}$$

The impedance of the fast-acting feedback force thus has mass and stiffness terms, together with a net negative resistance. When added to a passive harmonic oscillator (with impedance Z_p), the feedback force therefore both reduces the effective damping and modifies the natural resonant frequency. The combined system, $Z_{pf} = Z_p + Z_f$, has a net damping (Zweig, 1991)[23]

$$\delta_{pf} \approx \frac{\delta_p - \rho_f\psi_f}{\sqrt{1+\rho_f}}, \tag{17}$$

where $\delta_p > 0$ is the passive damping, $\rho_f \equiv K_f/K_p$ is the feedback strength relative to the passive stiffness, and $\psi_f \equiv \omega_p\tau_f$. The parameters K_p and $\omega_p \equiv 2\pi f_p$ are, respectively, the stiffness and resonant angular frequency of the original, passive oscillator. Similarly, the ratio of resonant frequencies becomes

$$f_{pf}/f_p \approx \sqrt{1+\rho_f}. \tag{18}$$

Consider now the constraints imposed by the near-invariance of the zero crossings of the impulse response. Figure 4 suggests that consistency with the data requires that the fractional change in resonant frequency, $|f_{pf} - f_p|/f_p$, due to the feedback force be small, say no more than roughly 10%. According to Eq. (18), this requirement imposes an upper bound on the strength of the feedback force: $\rho_f \lesssim 0.2$. Now to create a net negative damping, the feedback force must be strong enough that $\delta_{pf} < 0$. Analysis of the impedance $Z_{BM}(\beta)$ obtained using the inverse method suggests the rough estimate $\delta_{pf} \sim -\delta_p$ (Zweig, 1991). According to Eq. (17), this requires $\rho_f\psi_f \sim 2\delta_p$.[24] Recent attempts to fit experimental data obtained from the basal turns of the cochlea in passive preparations suggest that $\delta_p \gtrsim 0.1$ (e.g., Mammano and Nobili, 1993; Brass, 2000). Combining the equations yields the inequality

$$\psi_f \equiv \omega_p\tau_f \sim 2\delta_p/\rho_f \gtrsim 2(0.1)/0.2 \approx 1, \tag{19}$$

a constraint inconsistent with Eq. (13) and the assumption that the time delay is small compared to the oscillator period. In other words, the fast-time-delayed stiffness model cannot provide sufficient force to counteract the damping without shifting the resonant frequency of the system beyond the limits allowed by the data. In effect, the fast-time-delayed stiffness model therefore yields an impedance similar to the Z_a^{constant} of model $\mathcal{M}^<$, which fails to reproduce the near-invariance of fine time structure characteristic of the data.

The argument presented here does not, of course, rule out all time-delayed stiffness models, but only the simplest, in which the time delay is small compared to the period of the characteristic frequency. More elaborate models for negative damping—e.g., those that invoke additional tuning mechanisms, such as having the time delay depend strongly on position in the cochlea—remain viable. For example, if the time delay in Eq. (12) were to vary with position inversely with CF, so that $\tau_f(x)\omega_{CF}(x) \approx \pi/4$, then for frequencies $f \approx f_{CF}$ the impedance Z_f would contribute a nearly pure negative-resistance component and could presumably be arranged to produce only minor changes in the resonant frequency of the system.[25]

VI. SUMMARY AND DISCUSSION

Basilar-membrane and auditory-nerve responses to impulsive acoustic stimuli—whether measured directly in response to clicks or obtained indirectly using cross- or reverse-correlation and/or Fourier analysis—manifest a striking symmetry. A symmetry is something that stays the same while something else changes. In this case, the thing that changes is the intensity of the stimulus; the thing that stays the same is the phase of the oscillations in the response waveform (e.g., Kiang *et al.*, 1965; Goblick and Pfeiffer, 1969; Robles *et al.*, 1976; Carney and Yin, 1988; Ruggero *et al.*, 1992; de Boer and Nuttall, 1997; Recio *et al.*, 1998; Carney *et al.*, 1999; Lin and Guinan, 2000; de Boer and Nuttall, 2000; Recio and Rhode, 2000). In this paper, we have explored the origin and implications of this symmetry for cochlear mechanics. Applying the EQ-NL theorem (de Boer, 1997), we defined a family of linear cochlear models in which the strength of the active force generators is controlled by an intensity-dependent parameter, γ. We conjectured that invariance of fine time structure implies that as γ is varied the poles of the BM admittance remain within relatively narrow bands of the complex plane oriented perpendicular to the real frequency axis. Cochlear-model responses, computed by extending the model obtained by solution of the inverse problem in squirrel monkey at low sound levels (Zweig, 1991) with three different forms of the intensity dependence of the partition admittance, support the conjecture.

The models we employ here, which summarize the mechanics of the organ of Corti using equivalent point impedances and include only one-dimensional treatments of the full three-dimensional motion of the cochlear fluids, provide highly simplified representations of cochlear mechanics. By simplifying, however, we hope to ''eliminate the unnecessary so that the necessary may speak.''[26] Our intention, in other words, is not to exhibit models necessarily realistic in every detail, but rather to identify and explicate basic principles of cochlear function in the most transparent manner possible. Although obtained here using one-dimensional point-impedance models, our conclusions nevertheless apply in more realistic geometries as well. For example, one-dimensional models appear to capture, both qualitatively and semiquantitatively, the essential physics that gives rise to traveling-wave dispersion and glides (Shera, 2001). In addition, the impedances of the cochlear partition obtained as solutions to the inverse problem in long-wave, short-wave, and three-dimensional models are all in remarkable qualitative agreement (e.g., Zweig, 1991; de Boer, 1995a, b; de Boer and Nuttall, 1999). This general agreement among solutions to the inverse problem supports Zweig's (1991) conclusion that to reproduce the data, ''it is more important, in the hierarchy of approximations, to approximate . . . the impedance of the organ of Corti accurately than to work with the correct number of spatial dimensions.'' The success of our simple model, achieved despite Kolston's (2000) claim that ''three-dimensional fluid behavior should be regarded as a bare minimum in any quantitative description of cochlear mechanics,''[27] corroborates Zweig's remarks.

Physically, our conjecture implies that the local resonant frequencies of the cochlear partition are nearly independent of intensity. We demonstrate that this intensity *independence* of resonant frequencies is consistent with the well-known intensity *dependence* of the peak frequency of the BM transfer function, which shifts to lower frequencies at higher intensities (producing, at high intensities, the so-called ''half-octave shift''). We propose that, as with the glide (Shera, 2001), *the shift in best frequency arises globally*, through the intensity dependence of the dominant frequency of the driving pressure, *rather than locally*, through shifts in the local resonant frequencies of the partition. Our proposal thus resolves the long-standing paradox presented by measurements of mechanical click responses, which exhibit two seemingly contradictory features: On the other hand, the responses manifest the half-octave shift in best frequency with intensity; on the other, they exhibit near intensity-invariance of fine time structure.

Near-invariance of fine time structure requires that the feedback forces generated by the outer hair cells not significantly affect the natural resonant frequencies of the cochlear partition, which appear to vary by no more than roughly 10% over the full dynamic range of hearing. This requirement places strong constraints on the biophysical action of the cochlear amplifier or, more generally, on the mechanisms of cochlear dynamic-range compression, as characterized by the impedance $Z_a(\beta)$. In particular, we argue that the intensity invariance of fine time structure—combined with general principles, such as stability, local scaling, and causality—requires that in the region near CF the impedance $Z_a(\beta)$ must (1) be roughly spiral in form, (2) rotate clockwise with increasing frequency about a center with a negative real part, and (3) closely approach the real axis near the natural resonant frequency of the passive partition. This requirement appears inconsistent with models in which the OHCs modify the tonic stiffness of the cochlear partition, thereby effecting substantial changes in its resonant frequency (Allen, 1990, 1997). The requirement also suggests that tonic changes in OHC stiffness, whether mediated by somatic motor proteins (He and Dallos, 1999, 2000) or via the ciliary bundle (e.g., Howard and Hudspeth, 1988), have a relatively small effect on the total stiffness of the partition, at least for near-best-frequency stimuli in the basal turns of the cochlea. In this respect, our conclusions are consistent with current measurements, which suggest that the axial stiffness and the OHC is considerably smaller than the stiffness of the basilar membrane (Russell and Schauz, 1995; He and Dallos, 1999).

Our conclusions thus contradict many, if not most, cochlear models. Although most cochlear models are not manifestly nonlinear, they usually specify the equivalents of what we call $Z_{BM}(\beta)$ and $Z_p(\beta)$ (i.e., the impedances with and without contributions from force generation by OHCs). Since intensity variations appear to interpolate smoothly between these two extremes (de Boer and Nuttall, 2000), the qualitative behavior of a model's implicit intensity dependence can often be inferred from the relation between these two impedances. Our results indicate that to reproduce the invariance of the fine time structure of the impulse response, the resonant frequencies of $Z_{BM}(\beta)$ and $Z_p(\beta)$ need to be nearly identical (i.e., within roughly 10% of one another). However, plots of the effect of the cochlear amplifier on the BM admittance (Hubbard and Mountain, 1996) indicate that many cochlear models (e.g., Mountain *et al.*, 1983; Kolston *et al.*, 1990; Geisler, 1991; Hubbard, 1993) fail to satisfy this constraint, indicating that such models cannot reproduce the approximate invariance of response timing, as assessed either by varying intensity or by disabling the active mechanisms. Furthermore, our results rule out what is perhaps the most biophysically plausible mechanism so far proposed for the origin of negative damping, namely the fast-time-delayed stiffness model (Neely, 1983; Zweig, 1990). Although current cochlear models reproduce, to varying degrees, the form of empirical transfer functions measured in sensitive preparations near threshold, the problem they evidently leave unsolved is understanding the biophysical basis of an active feedback force that is strong enough to reverse the sign of the partition damping while leaving its resonant frequencies nearly unchanged.

ACKNOWLEDGMENTS

The author gratefully acknowledges many helpful discussions with and/or comments from Jont Allen, Egbert de Boer, Paul Fahey, John Guinan, Stephen Neely, William Peake, Robert Withnell, and George Zweig. This work was supported by Grant No. R01 DC03687 from the NIDCD, National Institutes of Health.

[1]Intensity-invariance of fine time structure, an excellent approximation at low and moderate sound-pressure levels (SPLs), breaks down in auditory-nerve responses at the highest sound levels. The data of Lin and Guinan (2000), for example, show clear evidence for phase reversals and other ''anomalies'' at click levels of 90 dB pSPL (peak-equivalent SPL) and above. Although species and methodological issues complicate the comparison, click responses measured on the basilar membrane show little evidence of comparable features, maintaining near-invariance of their zero crossings even at levels exceeding 115 pSPL (e.g., Recio and Rhode, 2000).

[2]In this paper, the term ''best frequency'' (BF) is used to locate the maximum of the BM frequency response, which may vary with intensity. The ''characteristic frequency'' (CF) is defined as the best frequency measured in the low-level linear limit. By definition, the CF is therefore independent of intensity.

[3]For an example illustrating the calculation of $\gamma(I/I_0)$ for a particular form of the transduction nonlinearity, see Appendix B of de Boer and Nuttall (2000).

[4]Given the normalized pole location $\zeta_\times \equiv \beta_\times + i\alpha_\times$, one can find the corresponding undamped resonant frequency and damping constant of the oscillator from the relations $f_p = f_{CF}|\zeta_\times|$ and $\delta_p = 2\alpha_\times/|\zeta_\times|$. Note that fixing the natural resonant frequency of the oscillator by moving its poles along lines of constant $\beta_\times$ requires changing both δ_p and f_p. Fractional changes in f_p, however, are generally small.

[5]Movement of the admittance poles along lines perpendicular to the real frequency axis yields exact invariance of fine time structure for the displacement response of the oscillator. For the velocity response, however, the invariance is only approximate. To see this, note that the velocity response of the oscillator has the form $v(\tau) \propto \cos(2\pi\beta_\times\tau + \phi)e^{-2\pi\alpha_\times\tau}$, where $\sin(\phi) = r/\sqrt{1+r^2}$ with $r \equiv \alpha_\times/\beta_\times$. The phase shift ϕ—and thus the fine time structure of the waveform (e.g., the position of its zero crossings)—therefore depends on $\alpha_\times$. Note, however, that this dependence on $\alpha_\times$ is weak (i.e., $\phi \ll 2\pi$ for the values $r \ll 1$ characteristic of tuned oscillators).

[6]In this paper the scaling variable β is defined as the model-independent ratio $f/f_{CF}(x)$, where $f_{CF}(x)$ is the characteristic frequency defined by the peak of the transfer function (see Note 2). Note, however, that in the model of cochlear mechanics defined by Eq. (9) (Zweig 1991), β refers to the ratio $f/f_r(x)$, where $f_r(x)$ is the undamped resonant frequency of the oscillator (i.e., the resonant frequency in the limit when the damping, δ, and stabilizing feedback force, ρ, are both negligible). The parameter values given in Note 8 imply that $f_{CF}(x)$ and $f_r(x)$ are everywhere proportional, with $f_r/f_{CF} \approx 1.03$. We have maintained the distinction between these two frequencies in all model calculations, but, for clarity of exposition, have ignored this small difference in the main text.

[7]Note that each of the infinite number of poles has a positive imaginary part. Despite creating a region of negative damping, the model is therefore stable at all frequencies (energy created at one location is absorbed at another). Equation (145) of Zweig (1991) gives an explicit expression for Y_{BM} in terms of its poles and their residues.

[8]This note describes the procedure used to determine the parameter values in the model admittance given in Eq. (9). The admittance $Y_{BM}(\beta)$ is first obtained as a function of ζ (or complex β) by analytic continuation into the complex frequency plane. [Recall from Note 6 that in this context the normalized frequency β is defined as the ratio $f/f_r(x)$.] Three constraining equations are then used to determine the three model parameters $\{\delta,\rho,\mu\}$. We specify (1) the imaginary part of one of the two closely spaced poles of $Y_{BM}(\zeta)$ and then require that (2) the real and (3) the imaginary parts of the second pole coincide with those of the first. More precisely, given $\alpha_* \equiv \mathrm{Im}\{\zeta_*\} > 0$, where ζ_* denotes the double pole of $Y_{BM}(\zeta)$, one determines the three parameters $\{\delta,\rho,\mu\}$; the real part of the double pole, $\beta_* \equiv \mathrm{Re}\{\zeta_*\}$; and the auxiliary variable a by solving the system of five simultaneous equations

$$\alpha_* = \delta/2 + a;$$

$$2\pi a\mu = 1;$$

$$a/\beta_* = \tan[2\pi(n/2 + \tfrac{3}{4}) - \beta_*/a];$$

$$\beta_*^2 = 1 - (\delta/2)^2 - a^2;$$

and

$$\rho = 2a[1 - (\delta/2)^2]^{1/2} e^{-\alpha_*/a}.$$

The solution for the auxiliary variable a is

$$a = (\alpha_* + \sqrt{\alpha_*^2 + c(1-\alpha_*^2)})/c,$$

where $c = 2 + x^{-2}$ and x is the solution to the equation

$$x^{-1} + \tan^{-1}(x) = 2\pi(n/2 + \tfrac{3}{4}),$$

obtained numerically. The values of $\{\delta,\rho,\mu\}$ can then be obtained by direct substitution. Evaluating the equations using the value $\alpha_* = \mathrm{Im}\{\zeta_*\} = 0.04$ adopted in the text (and taking $n=2$ for $\mu \approx 1\frac{3}{4}$) yields $\{\delta,\rho,\mu\} = \{-0.1024, 0.1175, 1.7450\}$. Finally, the proportionality constant in Eq. (9) for $Y_{BM}(\beta)$ was set equal to 1.

[9]The model parameter N, which determines the approximate number of wavelengths of the traveling wave on the basilar membrane in response to sinusoidal stimulation (Zweig *et al.*, 1976; Zweig, 1991), was given the value $N = 2.5$.

[10]The passive admittance thus has the form (6), with a proportionality constant of 1. In model $\mathcal{M}^{\approx}$, the damping constant δ_p was given the value $\delta_p = 0.32$; in model $\mathcal{M}^{<}$, introduced in Sec. III C 1, a slightly higher damping ($\delta_p = 0.42$) was needed to maintain model stability.

[11]Although we write ''model $\mathcal{M}^{\approx}$'' using the singular, $\mathcal{M}^{\approx}$ actually denotes an entire *family* of models, one for each value of γ.

[12]Recall that scaling relates properties of the mechanical transfer function to those of the traveling wave. In particular, mechanical transfer functions $T[f/f_{CF}(x)]$ measured as a function of f at fixed x also describe the traveling displacement wave as a function of x at fixed f. At fixed position, T is the transfer function; at fixed frequency, the traveling wave.

[13]Although qualitative agreement with the findings of de Boer and Nuttall (2000) remains strong, note that in the one-dimensional model used here the imaginary part of the partition impedance goes through zero at a value of β (≈ 1.03) closer to the location of the transfer-function peak than indicated by solutions to the inverse method obtained using two- and three-dimensional models (de Boer and Nuttall, 2000).

[14]Several of these poles located ''above CF'' are illustrated in Fig. 3 of Chap. VIII of Shera (1992) and in Fig. 5 of Zweig and Shera (1995).

[15]The admittance $y_{BM}(\tau;\gamma)$ represents the velocity response to a pressure impulse applied locally; it therefore jumps discontinuously to a nonzero value at $\tau = 0$ (see, e.g., Note 16 of Shera, 2001).

[16]To see that the principal poles of the model-$\mathcal{M}^{=}$ admittance are arrayed along a curve nearly perpendicular to the real-frequency axis, note that the equations in Note 8 yield $\beta_*^2 = 1 - \alpha_*^2 + \delta/2\pi\mu$, where $\zeta_* \equiv \beta_* + i\alpha_*$ denotes the location of the double pole of $Y_{BM}(\zeta)$ in the complex β plane. Since $\mu \approx 1\frac{3}{4}$, the quantity $|\delta|/2\pi\mu$ is typically much less than 1. Thus, $\beta_* \approx 1$ for values $\alpha_* \ll 1$. In other words, for $\alpha_* \ll 1$ the double pole lies approximately along the vertical line $\beta_* = 1$ at a distance α_* from the real axis. The small but systematic deviations from the vertical predicted by this analysis are evident in the trajectory shown in Fig. 5(c). [Recall that the line $\beta_* = 1$, for $\beta = f/f_r$, corresponds to the line $\beta_* = 1.03$, for $\beta = f/f_{CF}$ (see Note 6).]

[17]This explanation for the half-octave shift has been proposed independently by Carney (1999), who noted that intensity-dependent shifts in the temporal envelope of BM and auditory-nerve click responses, when combined with the intensity-independent frequency glide, can produce changes in the best frequency of the response.

[18]Although it characterizes the mechanical effects of local force generation by OHCs, the impedance Z_a should not be regarded as characterizing the ''cochlear amplifier.'' Cochlear amplification of traveling waves depends on both the active and passive mechanics and their interaction with the surrounding fluids over a fairly broad region of the cochlea.

[19]The suggestion that $Z_a(\beta)$ be represented as the sum of two components with this same qualitative form has been made earlier by Zweig (1990, 1991). In an effort to provide a biophysical basis for negative damping, Zweig suggested that $Z_a(\beta)$ be written as the sum of a fast- and a slow-acting time-delayed stiffness. In that model, the fast-time-delayed stiffness (delay much smaller than a period) provides negative damping and the slow-time-delayed stiffness (delay approximately $1\frac{3}{4}$ periods) provides the necessary frequency modulation by stabilizing the resulting oscillator. We discuss the fast-time-delayed stiffness model, and show that it yields an impedance Z_a^{constant} similar to that of model $\mathcal{M}^{<}$, in Sec. III C.

[20]For a passive oscillator of the form (7), the zero crossing of the reactance

$(\mathrm{Im}\{Z_p(\beta_0)\}=0)$ occurs at the value $\beta_0=|\zeta_\times|$, corresponding to the undamped resonant frequency of the oscillator (f_p).

[21]Reactance changes due to OHCs at other frequencies are not precluded: Indeed, as shown in Sec. III B, they are required by stability, local scaling, and causality.

[22]Note that the constraints of causality apply even though the real part of the impedance $Z_a(\beta)$ is negative.

[23]In deriving Eqs. (17) and (18) we have used the inequality $\psi_f=\omega_p\tau_f\ll 1$, an approximation equivalent to neglecting the mass term in Eq. (15).

[24]We have used the inequality $\rho_f\lesssim 0.2$ to approximate $\sqrt{1+\rho_f}$ as unity.

[25]This model for the origin of negative damping might be called the ''tuned-time-delayed stiffness model.''

[26]The quotation is from Hans Hoffmann (quoted in Efron and Tibshirani, 1993).

[27]Kolston may be referring here to recent suggestions from M theory that the universe we inhabit actually comprises ten spatial dimensions (see, e.g., Greene, 1999).

Allen, J. B. (**1990**). ''Modeling the noise damaged cochlea,'' in *Mechanics and Biophysics of Hearing*, edited by P. Dallos, C. D. Geisler, J. W. Matthews, M. A. Ruggero, and C. R. Steele (Springer, Berlin), pp. 324–331.

Allen, J. B. (**1997**). ''OHCs shift the excitation pattern via BM tension,'' in *Diversity in Auditory Mechanics*, edited by E. R. Lewis, G. R. Long, R. F. Lyon, P. M. Narins, C. R. Steele, and E. L. Hecht-Poinar (World Scientific, Singapore), pp. 167–175.

Bode, H. (**1945**). *Network Analysis and Feedback Amplifier Design* (Van Nostrand Reinhold, Princeton).

Brass, D. (**2000**). ''A macromechanical model of the guinea pig cochlea with realistic parameters,'' J. Acoust. Soc. Am. **107**, 894–907.

Carney, L. H. (**1999**). ''Temporal response properties of neurons in the auditory pathway,'' Curr. Opin. Neurobiol. **9**, 442–446.

Carney, L. H., McDuffy, M. J., and Shekhter, I. (**1999**). ''Frequency glides in the impulse responses of auditory-nerve fibers,'' J. Acoust. Soc. Am. **105**, 2384–2391.

Carney, L. H., and Yin, T. C. T. (**1988**). ''Temporal coding of resonances by low-frequency auditory nerve fibers: Single fiber responses and a population model,'' J. Neurophysiol. **60**, 1653–1677.

de Boer, E. (**1995a**). ''The inverse problem solved for a three-dimensional model of the cochlea. I. Analysis,'' J. Acoust. Soc. Am. **98**, 896–903.

de Boer, E. (**1995b**). ''The inverse problem solved for a three-dimensional model of the cochlea. II. Application to experimental data sets,'' J. Acoust. Soc. Am. **98**, 904–910.

de Boer, E. (**1997**). ''Connecting frequency selectivity and nonlinearly for models of the cochlea,'' Aud. Neurosci. **3**, 377–388.

de Boer, E., and Nuttall, A. L. (**1997**). ''The mechanical waveform of the basilar membrane. I. Frequency modulations ('glides') in impulse responses and cross-correlation functions,'' J. Acoust. Soc. Am. **101**, 3583–3592.

de Boer, E., and Nuttall, A. L. (**1999**). ''The inverse problem solved for a three-dimensional model of the cochlea. III. Brushing up the solution method,'' J. Acoust. Soc. Am. **105**, 3410–3420.

de Boer, E., and Nuttall, A. L. (**2000**). ''The mechanical waveform of the basilar membrane. III. Intensity effects,'' J. Acoust. Soc. Am. **107**, 1497–1507.

Efron, B., and Tibshirani, R. J. (**1993**). *An Introduction to the Bootstrap* (Chapman and Hall, New York).

Geisler, C. D. (**1991**). ''A cochlear model using feedback from motile outer hair cells,'' Hear. Res. **54**, 105–117.

Goblick, T. J., and Pfeiffer, R. R. (**1969**). ''Time-domain measurements of cochlear nonlinearities using combination click stimuli,'' J. Acoust. Soc. Am. **46**, 924–938.

Greene, B. (**1999**). *The Elegant Universe—Superstrings, Hidden Dimensions, and the Quest for the Ultimate Theory* (Norton, New York).

Gummer, A. W., Smolders, J. W. T., and Klinke, R. (**1987**). ''Basilar membrane motion in the pigeon measured with the Mössbauer technique,'' Hear. Res. **29**, 63–92.

He, D. Z. Z., and Dallos, P. (**1999**). ''Somatic stiffness of cochlear outer hair cells is voltage dependent,'' Proc. Natl. Acad. Sci. U.S.A. **96**, 8223–8228.

He, D. Z. Z., and Dallos, P. (**2000**). ''Properties of voltage-dependent somatic stiffness of cochlear outer hair cells,'' J. Assoc. Res. Otolaryngol. **1**, 46–813.

Howard, J., and Hudspeth, A. J. (**1988**). ''Compliance of the hair bundle associated with gating of mechanoelectrical transduction channels in the bullfrog's saccular hair cell,'' Neuron **1**, 189–199.

Hubbard, A. E. (**1993**). ''A traveling-wave amplifier model of the cochlea,'' Science **259**, 68–71.

Hubbard, A. E., and Mountain, D. C. (**1996**). ''Models of the cochlea,'' in *Auditory Computation*, edited by H. L. Hawkins, T. A. McMullen, A. N. Popper, and R. R. Fay (Springer, New York), pp. 62–120.

Kiang, N. Y. S., and Moxon, E. C. (**1974**). ''Tails of tuning curves of auditory-nerve fibers,'' J. Acoust. Soc. Am. **55**, 620–630.

Kiang, N. Y. S., Watanabe, T., Thomas, E. C., and Clark, L. F. (**1965**). *Discharge Patterns of Single Fibers in the Cat's Auditory Nerve* (MIT, Cambridge, MA).

Kolston, P. J. (**2000**). ''The importance of phase data and model dimensionality to cochlear mechanics,'' Hear. Res. **145**, 25–36.

Kolston, P. J., Viergever, M. A., de Boer, E., and Smoorenburg, G. F. (**1990**). ''What type of force does the cochlear amplifier produce?'' J. Acoust. Soc. Am. **88**, 1794–1801.

Liberman, M. C. (**1978**). ''Auditory-nerve response from cats raised in a low-noise chamber,'' J. Acoust. Soc. Am. **63**, 442–455.

Lin, T., and Guinan, J. J. (**2000**). ''Auditory-nerve-fiber responses to high-level clicks: Interference patterns indicate that excitation is due to the combination of multiple devices,'' J. Acoust. Soc. Am. **107**, 2615–2630.

Mammano, F., and Nobili, R. (**1993**). ''Biophysics of the cochlea: Linear approximation,'' J. Acoust. Soc. Am. **93**, 3320–3332.

Moller, A. R. (**1977**). ''Frequency selectivity of single auditory-nerve fibers in response to broadband noise stimuli,'' J. Acoust. Soc. Am. **62**, 135–142.

Mountain, D. C., Hubbard, A. E., and McMullen, T. A. (**1983**). ''Electromechanical processes in the cochlea,'' in *Mechanics of Hearing*, edited by E. de Boer and M. A. Viergever (Martinus Nijhoff, The Hague), pp. 119–126.

Neely, S. T. (**1983**). ''The cochlear amplifier,'' in *Mechanics of Hearing*, edited by E. Boer and M. A. Viergever (Martinus Nijhoff, The Hague), pp. 111–118.

Papoulis, A. (**1977**). *Signal Analysis* (McGraw-Hill, New York).

Recio, A., and Rhode, W. S. (**2000**). ''Basilar membrane responses to broadband stimuli,'' J. Acoust. Soc. Am. **108**, 2281–2298.

Recio, A., Rich, N. C., Narayan, S. S., and Ruggero, M. A. (**1998**). ''Basilar-membrane responses to clicks at the base of the chinchilla cochlea,'' J. Acoust. Soc. Am. **103**, 1972–1989.

Rhode, W. S. (**1971**). ''Observations of the vibration of the basilar membrane in squirrel monkeys using the Mössbauer technique,'' J. Acoust. Soc. Am. **49**, 1218–1231.

Rhode, W. S., and Recio, A. (**2000**). ''Study of mechanical motions in the basal region of the chinchilla cochlea,'' J. Acoust. Soc. Am. **107**, 3317–3332.

Robles, L., Rhode, W. S., and Geisler, C. D. (**1976**). ''Transient response of the basilar membrane measured in squirrel monkeys using the Mössbauer effect,'' J. Acoust. Soc. Am. **59**, 926–939.

Ruggero, M. A., Rich, N. C., and Recio, A. (**1992**). ''Basilar membrane responses to clicks,'' in *Auditory Physiology and Perception*, edited by Y. Cazals, K. Horner, and L. Demany (Pergamon, Oxford), pp. 85–91.

Russell, I., and Schauz, C. (**1995**). ''Salicylate ototoxicity: Effects on the stiffness and electromotility of outer hair cells isolated from the guinea pig cochlea,'' Aud. Neurosci. **1**, 309–319.

Shera, C. A. (**1992**). ''Listening to the Ear,'' Ph.D. thesis, California Institute of Technology.

Shera, C. A. (**2001**). ''Frequency glides in click responses of the basilar membrane and auditory nerve: Their scaling behavior and origin in traveling-wave dispersion,'' J. Acoust. Soc. Am. **109**, 2023–2034.

Siebert, W. M. (**1968**). ''Stimulus transformations in the peripheral auditory system,'' in *Recognizing Patterns*, edited by P. A. Kolers and M. Eden (MIT, Cambridge), pp. 104–133.

Sondhi, M. M. (**1978**). ''Method for computing motion in a two-dimensional cochlear model,'' J. Acoust. Soc. Am. **63**, 1468–1477.

Zweig, G. (**1976**). ''Basilar membrane motion,'' in *Cold Spring Harbor Symposia on Quantitative Biology, Volume XL, 1975* (Cold Spring Harbor Laboratory, Cold Spring Harbor, NY), pp. 619–633.

Zweig, G. (**1990**). ''The impedance of the organ of Corti,'' in *Mechanics*

and Biophysics of Hearing, edited by P. Dallos, C. D. Geisler, J. W. Matthews, M. A. Ruggero, and C. R. Steele (Springer, Berlin), pp. 362–369.
Zweig, G. (**1991**). ''Finding the impedance of the organ of Corti,'' J. Acoust. Soc. Am. **89**, 1229–1254.
Zweig, G., Lipes, R., and Pierce, J. R. (**1976**). ''The cochlear compromise,'' J. Acoust. Soc. Am. **59**, 975–982.
Zweig, G., and Shera, C. A. (**1995**). ''The origin of periodicity in the spectrum of evoked otoacoustic emissions,'' J. Acoust. Soc. Am. **98**, 2018–2047.